

This paper should be cited as:

Morales-Marin L, French JR, Burningham H, Evans C, Burden E (2021) Simulating seasonal to multi-decadal variation in lake thermal response to meteorological forcing using the UCLAKE 1-dimensional model code. *Limnologia* 88, 125874

Simulating seasonal to multi-decadal variation in lake thermal response to meteorological forcing using the UCLAKE 1-dimensional model code

Luis A. Morales-Marín^{a,1}, Jon R. French^a, Helene Burningham^a, Chris Evans^b,
Annette Burden^b

^a*UCL Department of Geography, University College London, Gower Street, London WC1E 6BT, UK*

^b*Centre for Ecology & Hydrology, Environment Centre Wales, Deiniol Road, Bangor LL57 2UW, UK*

Abstract

Lake temperature responses to climate forcing are of interest on account of the important linkages between water temperature and ecosystem processes. This paper describes a new 1-dimensional (1D) numerical model code and its application to investigations of multi-scale linkages between the vertical temperature structure and meteorological forcing. UCLAKE is implemented as highly portable open-source software, based on computationally efficient algorithms, and able to resolve sub-daily (e.g. hourly) dynamics while retaining the efficiency to simulate multi-decadal time scales.

A UCLAKE model is calibrated and validated against thermistor profile time series for a small upland lake in North Wales, UK. Some of the challenges in 1D model calibration are explored and a sensitivity analysis reveals a dependence of optimal parameter set values on water column depth and time. An exploratory 52-year hindcast simulation demonstrates the computational efficiency of UCLAKE for multi-decadal studies of trends in lake temperature that vary with depth. A supplementary application of UCLAKE to Windermere, in the English Lake District, demonstrates its performance for larger and deeper lakes.

1. Introduction

There is considerable interest in the response of lakes to climate change, especially in relation to warming trends and their implications for ecosystem functions (Cohen et al., 2016; Winslow et al., 2017). Lake water temperature is an especially

Email addresses: lmoralesma@gmail.com (Luis A. Morales-Marín), j.french@ucl.ac.uk (Jon R. French), h.burningham@ucl.ac.uk (Helene Burningham), cev@ceh.ac.uk (Chris Evans), anrd@ceh.ac.uk (Annette Burden)

¹Now at Global Institute for Water Security, University of Saskatchewan, 11 Innovation Boulevard, Saskatoon, SK S7N 3H5

important variable since it typically exhibits a sensitive response to meteorological forcing and exerts a strong influence on lake biology (Livingstone and Dokulil, 2001; Woolway et al., 2016). There is abundant observational evidence for an increase in surface temperatures that tracks atmospheric warming over the last few decades (Adrian et al., 2009; O'Reilly et al., 2015; Woolway et al., 2017). The thermal response of the hypolimnion, by contrast, is much more variable and depends on lake size, morphology, and exposure to wind forcing (Dokulil et al., 2006; Rösner et al., 2012; Kraemer et al., 2015; Morales-Marin et al., 2017).

Empirical studies have tended to focus on lakes for which long monitoring datasets are available (e.g., Austin and Coleman, 2007; Hampton et al., 2008). However, the multi-decadal temperature profile time series needed to understand more complex climate-driven changes in lake thermal structure are available for only a few lakes and observations are increasingly being supplemented by modelling (Vinçon-Leite et al., 2014; Valerio et al., 2015).

Although 3D models are required to resolve some of the processes that determine lake responses to climate warming (e.g., Woolway and Merchant, 2018; Zhong et al., 2019), 1D schemes are appropriate when the object of study is the energy exchange with the atmosphere and when the vertical gradients are significantly larger than the horizontal ones (Perroud et al., 2009). 1D models generally adopt either an eddy diffusivity or an energy budget approach. Eddy diffusivity models (e.g. MINLAKE (Riley and Stefan, 1988; Yao et al., 2014) and QUALAKE-DOT (Antonopoulos and Gianniou, 2003)) solve an advection-diffusion equation, with meteorological boundary conditions imposed at the water surface. A homogeneous distribution in the epilimnion is assumed and the turbulent diffusion coefficient is estimated empirically (e.g., Orlob and Selna, 1970) or via an analytical function (e.g., Henderson-Sellers, 1984). Energy budget models (e.g. DYSREM, (Imberger and Patterson, 1981) and MyLake (Saloranta and Andersen, 2007)) include a turbulence closure scheme in which the heat flux between vertical layers of the water column is related to the turbulent kinetic energy due to wind forcing (Hostetler et al., 1993).

It has been argued (Mooij et al., 2010) that we now have such a variety of lake models that further development risks 'reinventing the wheel'. However, only a subset of model codes are freely available, including Simstrat (Goudsmit et al., 2002) and the General Lake Model (GLM) (Hipsey et al., 2014). Other codes are available but implemented in proprietary languages (e.g. MYLAKE; Saloranta and Andersen, 2007), require supporting libraries (e.g. GOTM; Burchard et al., 2006), or are intended for specialised applications, such as resolving lake effects in numerical weather predictions (e.g. FLAKE; Mironov et al., 2010). Within this spectrum of models, there is still a niche for simple codes that are free from external software dependencies, capable of being validated with a minimal set of calibration parameters in data-sparse locations, and efficient enough to permit simulation at timescales of decades to centuries.

In this paper, we describe a new 1D eddy-diffusivity model, UCLAKE (University College London lake model), that is computationally efficient and is imple-

mented with flexible time steps to allow investigations ranging from the effects of sub-daily meteorological forcing to centennial-scale responses to climate variability and change. UCLAKE is open source and free of external software or library dependencies. We calibrate and validate UCLAKE against observational data for an upland lake, Llyn Conwy, in North Wales, UK. Sensitivity analysis is performed to elucidate some of the challenges in calibration. Comparative analysis shows UCLAKE to be slightly faster and simpler to implement than GLM (Hipsey et al., 2014), while offering similar or better performance against observational data. An exploratory 52-year hindcast simulation for Llyn Conwy demonstrates the computational efficiency of the UCLAKE model code for the analysis of multi-decadal trends in lake water temperature. To assess its performance for a deeper lake, UCLAKE was also calibrated for Windermere, in the English Lake District.

2. Model description

2.1. Overview

UCLAKE solves the 1D advection-diffusion equation, here given as

$$\frac{\partial T(z, t)}{\partial t} = \frac{1}{A(z)} \frac{\partial}{\partial z} (A(z) K z(z, t) \frac{\partial T}{\partial z}) - \frac{1}{\rho C_p A(z)} \frac{\partial A(z) q(z, t)}{\partial z} \quad (1)$$

where z is the water depth (m) measured downward from water surface ($z = 0$) to the bottom ($z = h$); t is the time (s), $T(z, t)$ is the water temperature ($^{\circ}\text{C}$), $A(z)$ is the horizontal area at the mid-point of a layer (see Ala_i in Figure 1a); $Kz(z, t)$ is the turbulent diffusion coefficient ($\text{m}^2 \text{s}^{-1}$), $q(z, t)$ describes the net rate of heat generation (W m^{-2}) due to radiation absorption within the water column, and C_p is the specific heat of water.

Equation 1 is solved on the assumption that the lake is comprised of multiple homogenous horizontal layers (Figure 1a). The equation is resolved using fully implicit finite differences. This reduces the discrete domain (i.e. the layers) to a linear equation system, the tri-diagonal coefficient matrix of which is then efficiently inverted using the Thomas algorithm (Press et al., 2007) to yield water temperature at the centre of each layer at every time step.

The stability condition for 1D advection-diffusion models dictates that numerical calculations will be stable if $\frac{\delta^2}{2Kz\Delta t} \leq 1$ (Ryan and Harleman, 1973). Since the maximum value of Kz varies continuously, adaptive variation of Δt is implemented to ensure numerical stability at every step.

2.1.1. Water surface boundary conditions

Boundary conditions for Equation 1 are imposed at the surface in the form of the net heat flux and the wind shear stress. The net downward heat flux, $q(z, t)$, is computed as

$$q(z) = \begin{cases} Hn = (1-r)Hs + Hl - He - Hc & \text{if } z = 0 \text{ (uppermost layer)} \\ (1-\beta_s)Hs \exp(-\eta z) & \text{if } z > 0 \text{ (lower layers)} \end{cases} \quad (2)$$

where Hn is the net heat flux at the water surface (W m^{-2}); Hs is the short-wave irradiation measured at the water surface (W m^{-2}); Hl is the long-wave radiation (W m^{-2}); He is the evaporative heat flux, Hc is the sensible heat (W m^{-2}), r is the short-wave reflectivity, β_s is the fraction of short-wave irradiation absorbed at the water surface and η is the extinction coefficient of the surface net head budged for lower layers (m^{-1}).

Long-wave radiation, Hl , is computed as the balance between the radiation emitted by the water surface (Hl_{ro}) and the net radiation received from the atmosphere and the clouds, Hl_{ra} , given as

$$Hl = Hl_{ra} - Hl_{ro} \quad (3)$$

Hl_{ro} is estimated as $Hl_{ro} = \varepsilon_w \sigma T_w^4$ where T_w is the water surface temperature in K, σ is the Stefan-Boltzmann constant ($5.67 \times 10^{-8} \text{ W m}^{-2} \text{ K}^{-4}$) and ε_w is the emissivity for water (~ 0.97). Hl_{ra} is estimated from $Hl_{ra} = Hl_{ri}(1 - A_L)$, where A_L is the long wave reflectivity constant, which is taken to be 0.03 (Henderson-Sellers, 1984). The incoming radiation from the atmosphere and clouds is given by $Hl_{ri} = \varepsilon_a \sigma T_a^4$ where T_a is the air temperature in K and the emissivity ε_a is

$$\varepsilon_a = \begin{cases} 0.87 - \frac{n}{D}(0.175 - 29.92 \times 10^{-6} \psi e_{sa}) + 2.693 \times 10^{-5} e_{sa} & \text{if } \frac{n}{D} \leq 0.4 \\ 0.84 - \frac{n}{D}(0.100 - 9.973 \times 10^{-6} \psi e_{sa}) + 3.491 \times 10^{-5} e_{sa} & \text{if } \frac{n}{D} \geq 0.4 \end{cases} \quad (4)$$

In the above expressions for ε_a , $\frac{n}{D}$ is the fractional sunshine duration where n is the number sunshine hours and D is the number of hours per day, and ψ is the relative humidity given as

$$\psi = \frac{\text{actual vapour pressure}}{\text{saturated vapour pressure}}$$

and the saturated vapour pressure is given by the empirical equation $e_{sa} = 2.171 \times 10^{10} \exp^{-4157/(T-33.41)}$ (N m^{-2}), where T is the air temperature in K (Glanz et al., 1973).

The evaporative heat flux, He , represents the heat energy loss due to water evaporation and is determined from

$$He = L_v \rho E; \quad (5)$$

where the latent heat of vaporisation is given as (Huber and Harleman, 1968) $L_v = 1000[2500.9 - 2.365(T_w - 273)]$ (J kg^{-1}). The dependence of water density, ρ (kg m^{-3}), on temperature is approximated as $\rho = 1000[1.0 - 6.63 \times 10^{-6}(T - 277)^2]$. E is the evaporative flux (m s^{-1}), given as $E = f(W)(e_{sw} - e_a)$ where

$f(W) = a + bW$ is a function of wind velocity (W), and a and b are constants. UCLAKE implements five different formulae for the estimation of E . The default option is the widely used Penman equation (Penman, 1948) $E = 0.44 \times 10^{-10}(1 + 0.537W_2)(e_{sw} - e_a)$ in m s^{-1} , where W_2 is the wind speed measured 2 m above the surface, e_{sw} is the saturated vapour pressure at the water temperature and e_a is the actual vapour pressure at the temperature of the air.

The sensible heat flux, H_c , is related to He through the Bowen ratio (β) (Henderson-Sellers, 1984) as

$$H_c = 0.61 \times 10^{-3} p H_e \left(\frac{T_w - T_a}{e_{sw} - e_a} \right) \quad (6)$$

where p is the atmosphere pressure (N m^{-2}) and T_a and T_w are air and water temperature respectively.

Turbulent kinetic energy, E_k due to wind shear (Ford and Stefan, 1980) is computed from

$$E_k = A_s C \hat{w} \tau \quad (7)$$

where C is a wind sheltering coefficient, A_s is the water surface area (m^2) and $\hat{w} = \sqrt{\tau/\rho}$ is the friction velocity (m s^{-1}). $\tau = \rho_a C_D W^2$ is the shear stress, where ρ_a is air density (kg m^{-3}), C_D is the drag coefficient and W is the wind speed (m s^{-1}). In UCLAKE, C_D is determined using the following expression originally derived for oceans (Wu, 1982)

$$C_D = \begin{cases} 1.25W^{-0.5} \times 10^{-3} & W \leq 1 \text{ m s}^{-1} \\ 0.5W^{0.5} \times 10^{-3} & 1. < W < 15 \text{ m s}^{-1} \\ 2.6 \times 10^{-3} & W \geq 15 \text{ m s}^{-1} \end{cases} \quad (8)$$

2.1.2. Water mass balance

Water balance calculation is important, not least because time variation in water depth influences the ability of wind to deepen the mixed layer. UCLAKE includes the water fluxes arising from rainfall and evaporation, groundwater and surface inflows and outflows. Rainfall, R (m h^{-1}), is a measured quantity usually obtained from a suitably close meteorological station, whilst evaporation, E (m s^{-1}), is calculated using one of several standard formulae (see above). Both quantities are assumed to be homogeneously distributed across the water surface and only affect the water balance of the uppermost layer, expressed as:

$$\frac{V_1^{t+1} - V_1^t}{\Delta t} = +(R - E) A l a_1^t; \quad (9)$$

where V_1 is the volume (m^3) of the uppermost layer.

Layer geometry (area, thickness and volume; Figure 1a) is adjusted at each time step in accordance with the computed net water balance. Layers that exceed the maximum layer thickness are divided equally into two new layers. Layers that

thin below a minimum value are merged with the layer just above or below. The updated geometry is used at the next time step.

2.1.3. Turbulent diffusion coefficient

Following Henderson-Sellers (1985), the turbulent diffusion coefficient, Kz , at the mixed layer depth (h_{mix}) is calculated as

$$Kz_0 = \frac{\hat{w}^2}{uk^*} \exp -zk^* \quad 0 \leq z \leq h_{mix} \quad (10)$$

where $k^* = 4.7(f/\hat{w})$ is the decay constant of \hat{w} , f is the Coriolis coefficient and $u = 22.6\hat{w}w^{-0.1}/\sin(lat)$ is related to wind velocity, w , (m s^{-1}), and lat is the latitude (in radians).

Kz below the mixing layer is calculated, after Munk and Anderson (1948), as

$$Kz = Kz_0(1 + \alpha R_i^\gamma)^{-\beta} \quad h_{mix} < z \leq h \quad (11)$$

where α , γ and β are constants that usually take values of 37, 2 and 1 respectively (Henderson-Sellers, 1985). R_i is the Richardson number

$$R_i = \frac{-1 + \sqrt{1 + \frac{40N^2\kappa^2z^2}{\hat{w}^2 \exp -2k^*z}}}{20} \quad (12)$$

where $\kappa = 0.4$ is the Von Karman constant and $N^2 = -(g/\rho)(\partial\rho/\partial z)$ is the Brunt-Vaisala frequency.

Given that the above expressions provide only an approximation of the depth-variation in Kz , it is necessary to constrain Kz in the layers below the mixed layer using a maximum diffusion coefficient that must be obtained through calibration.

2.1.4. Model implementation

Some open-source lake model codes require the use of proprietary software, such as Matlab (e.g., Saloranta and Andersen, 2007), which can be restrictive. Like GLM (Hipsey et al., 2014), UCLAKE is coded in C, which offers a good combination of performance and portability across the main computer operating systems. The program is structured into routines that provide input/output functionality (Figure 1b), and compute the various terms in the 1D advection-diffusion equation (Equation 1). Run times depend on the choice of time step and the discretisation used but, as a rough guide, a 20-layer simulation of 1 year duration at an hourly time step can be accomplished in less than 3 minutes of cpu time on a single 3.4 GHz Intel Xeon processor core. This makes UCLAKE particularly suitable for sensitivity analyses using large ensembles of runs or lake physical responses to climate forcing at multi-decadal time scales. The code is also simple enough for it to be used as an educational tool. The source code is being made available under an open source licence via the GitHub repository (link to be provided). Appendix 1 presents a comparative analysis showing UCLAKE to be slightly faster and simpler to implement than GLM (Table A.5), while offering similar or better performance against observational data (Figure A.16 and A.17).

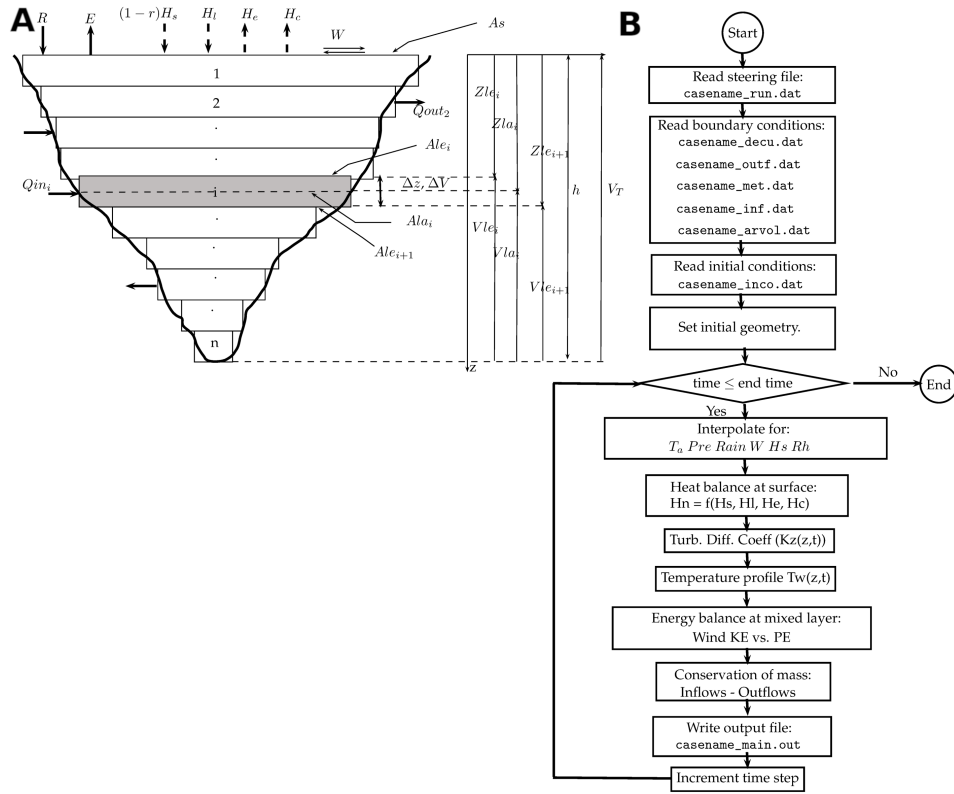


Figure 1: a) Computational discretization of a lake domain in UCLAKE. Most terms are explained in the text, but As is the actual lake surface area; Ala_i is the actual area at the mid-point of model layer i ; and Ale_i is the area of level i in the the discretization scheme. Z and V similarly refer to the elevation and volume of the layers. b) UCLAKE program structure.

3. Validation case study: Llyn Conwy, Wales, UK

3.1. Site details

The initial model validation was performed for Llyn Conwy, a small oligotrophic upland lake with a surface area of 0.4 km^2 and situated 450 m above mean sea level in North Wales, UK (Figure 2). The lake is located within a peat-dominated plateau (Patrick and Stevenson, 1986) and is exposed to energetic wind forcing, predominantly from the southwest. Mean and maximum water depth are approximately 7.7 and 22.0 m and the bathymetry is characterised by a deep north-central basin flanked by shallower bays to the south and east. Inflow is largely distributed around the shoreline via seepage and surface runoff from the blanket peat. Although natural, the lake is used as a source of drinking water and its level is regulated by an artificial sill at its outflow.

Selection of Llyn Conwy was guided by the availability of meteorological and limnological data acquired by the Centre for Ecology and Hydrology (CEH) as part of broader study of biogeochemical cycling in the Conwy catchment. Mean annual precipitation is approximately 2300 mm and mean annual temperature is 8°C (Austnes et al., 2010). A CEH automatic weather station within the catchment between 2006 and 2008 recorded mean annual wind speeds of 9.3 m s^{-1} , with peak hourly wind speeds exceeding 30 m s^{-1} on several occasions. Water temperatures were recorded by a vertical string of 10 platinum resistance thermometers (PRT) at 2 m intervals attached to a monitoring buoy moored in the deepest part of the lake (Figure 2).

3.2. Model Setup

Analysis of precipitation and runoff records indicates that about 85% of the annual water precipitation becomes runoff, of which nearly 70% (approximately $1.2 \times 10^6 \text{ m}^3 \text{ yr}^{-1}$) flows into the lake. Lake water level varies by no more than about $\pm 1 \text{ m}$ throughout a typical year (drinking water abstraction is small). Given the small variation in water level and small magnitude of the inflows and outflows relative to the total water volume, only the incoming rainfall and the outgoing evaporation at the water surface are included in the model water balance calculations reported here.

Parameter values used in calibration and validation are summarised in Table 1. For calibration purposes, fixed values were used for most of the parameters, taken from appropriate literature sources. Three parameters were adjusted in order to calibrate model output against observed data: maximum turbulent diffusion coefficient in the hypolimnion ($K_{z_{max}}$), the wind sheltering coefficient (C), and the extinction coefficient (η). Calibration was accomplished using 80 sets of parameter values, using a Monte-Carlo approach (Beven and Freer, 2001). The model was evaluated following three objective functions: the root mean square error (RMSE), relative mean absolute error (RMAE) and the Nash-Sutcliffe efficiency coefficient (NSE) (Nash and Sutcliffe, 1970) as a measure of overall performance.

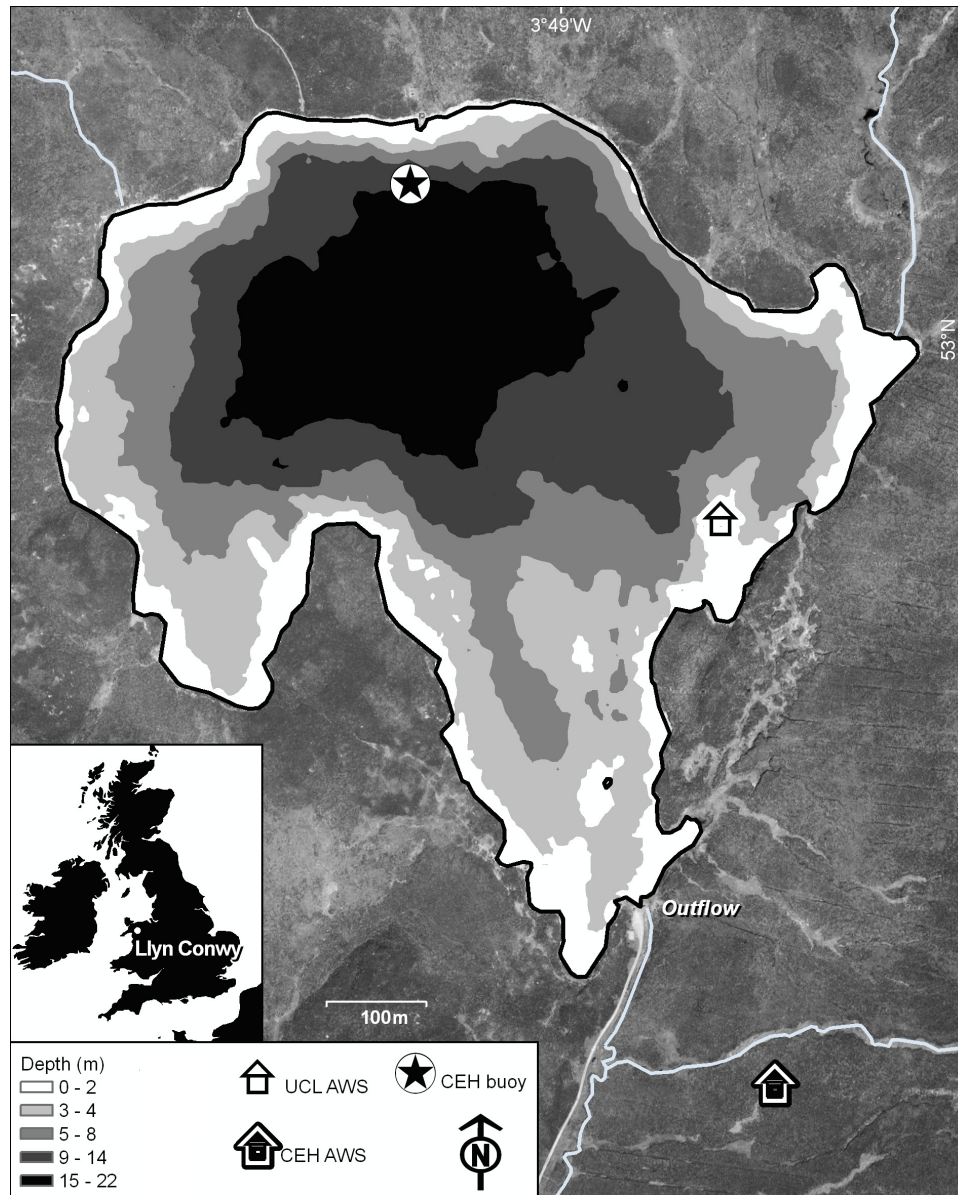


Figure 2: Location, bathymetry of Llyn Conwy and data acquisition locations (CEH data buoy and UCL Automatic Weather Station). Depth contours in m.

Table 1: Parameter values used in *UCLAKE*, with values used in Llyn Conwy case study. Parameters in bold were adjusted within the indicated ranges for model calibration.

Parameter	Symbol	Values	Units	Literature Source
Max. layer thickness	δ_{max}	1.5	m	[5]
Min. layer thickness	δ_{min}	0.5	m	[5]
Max. hypolim. turb. diff. coeff.	Kz_{max}	9.95e-7 - 1.00e-4	$m^2 s^{-1}$	—
Long-wave albedo	α	0.04	—	[4]
Short-wave reflectivity	r	0.08	—	[1]
Wind sheltering coefficient	C	0.1 - 1.0	—	—
Emissivity of water	ϵ	0.972	—	[2]
Solar rad. fract. absor. in top layer	β_s	0.5	—	[6]
Extinction coefficient	η	0.1 - 2.0	m^{-1}	—
Constant in Equation 11	α	37	—	[3]
Constant in Equation 11	β	1	—	[3]
Constant in Equation 11	γ	2	—	[3]
Molecular diffusion coefficient	Kz_{mol}	1.2×10^{-7}	$m^2 s^{-1}$	[6]
Latitude	Lat	53	$^{\circ}$	—
Initial number of layers	n_{lay0}	25	—	—
Initial water surface level	Lev_{ws}	0.0	m	—
Bottom depth	Lev_{bot}	21.0	m	—

[1] Patten et al. (1975); [2] Imberger and Patterson (1981); [3] Henderson-Sellers (1985); [4] Nakamura and Hayakawa (1991); [5] Hondzo and Stefan (1993); [6] Bonnet et al. (2000)

3.3. Exploratory multi-decadal hindcast simulation

To demonstrate the ability of *UCLAKE* to model long-term variation in lake thermal structure, a 52 year (1948-2000) hindcast simulation was also performed for Llyn Conwy. This was forced by meteorological data acquired from the near-real-time Global Land Data Assimilation Scheme (GLDAS) data product developed at by NASA Goddard Space Flight Center and the NOAA National Center for Environmental Prediction (Rodell et al., 2004). GLDAS uses relevant remotely-sensed and in-situ observations within a land data assimilation framework to simulate meteorological variables on a 0.25° grid at a three-hour time step.

GLDAS data for the cell that contains the Llyn Conwy catchment were down-scaled and bias corrected. The empirical-statistical downscaling and error correction method (e.g., Themeßl et al., 2012; Fang et al., 2015) was adopted using meteorological observations from the UK Met Office network. This adjusts the mean, the standard deviation and the quantiles of the GLDAS data and preserves the extremes. The downscaled meteorological variables were re-sampled to a 1-hour model time step to force multi-decadal simulations of lake temperature. No validation data are available for this simulation and the results are purely illustrative of the ability of *UCLAKE* to undertake efficient multi-decadal simulation, including for future scenarios.

4. Deep lake case study: Windermere, UK

The performance of UCLAKE for simulation of deeper lakes was evaluated through a supplementary investigation of Windermere, in the English Lake District, UK (Figure 3). Windermere comprises two distinct sub-basins and only the south basin was simulated here. This has a surface area of 63 km^2 , holds a water volume of $11.3 \times 10^7 \text{ m}^3$ with a maximum depth of about 43 m . Windermere is a warm monomictic lake that stratifies during spring and summer, and is characterized by water temperature overturns during autumn and winter. The climate is mild, with air temperatures between $-6 \text{ }^\circ\text{C}$ in winter and $25 \text{ }^\circ\text{C}$ in summer, and wind speeds generally less than 15 m s^{-1} . UCLAKE was implemented to simulate the water temperature dynamics in the south basin for the years 2008 through 2011. Model setup was based on high resolution bathymetry and forced using hourly meteorological data (Jones and Feuchtmayr, 2017). Validation was performed against observed hourly water temperature time series at 12 water depths from 1 to 35 m (Jones and Feuchtmayr, 2017).

5. Results

5.1. Calibration of Llyn Conwy model

Calibration runs were forced by meteorological data for November 2006 to October 2007 (Figure 4). The first step was to compare the simulated and observed temperature at three different levels within the water column: water surface; mid-depth; and bottom layer. At the water surface (Figure 5), 95% of parameter value combinations achieve $NSE > 0.94$. Model performance is weaker at mid-depth (Figures 6) and at the bottom (Figures 7). Even here, however, values of NSE are still good with about 95% of the parameter value combinations yielding $NSE > 0.5$. The spread of the model performance at mid-depth and at the bottom (about $-1.5 < NSE < 1.0$) is larger than at the water surface (about $0.88 < NSE < 1.0$). $RMSE < 0.8$ and $RMAE < 9$ were found at all water depths.

Table 2 shows the optimal parameter set values at each relative water depth. For both the mid- and bottom layers (Figures 6 and 7, respectively), the worst model performance arises for those parameter sets that include values of Kz_{max} under $1.5 \times 10^{-5} \text{ m}^2 \text{ s}^{-1}$. This can be explained by the fact that the energy dissipation carried out by the model at the rate specified by Kz_{max} below the mixed layer is overestimated for periods where there is stratification.

Given that the optimum parameter values vary as a function of the water depth (Table 2), it is desirable to obtain a single set that provides the best overall performance over the water column as a whole. Hondzo and Stefan (1993) implemented a formulation in which the water temperature at each layer weighted by its volume, and the cumulative sum divided by the total lake volume. Basin geometry exerts an influence and, in the present case, it was found that this approximation places too much weight on the upper layers and too little on the lower layers. As

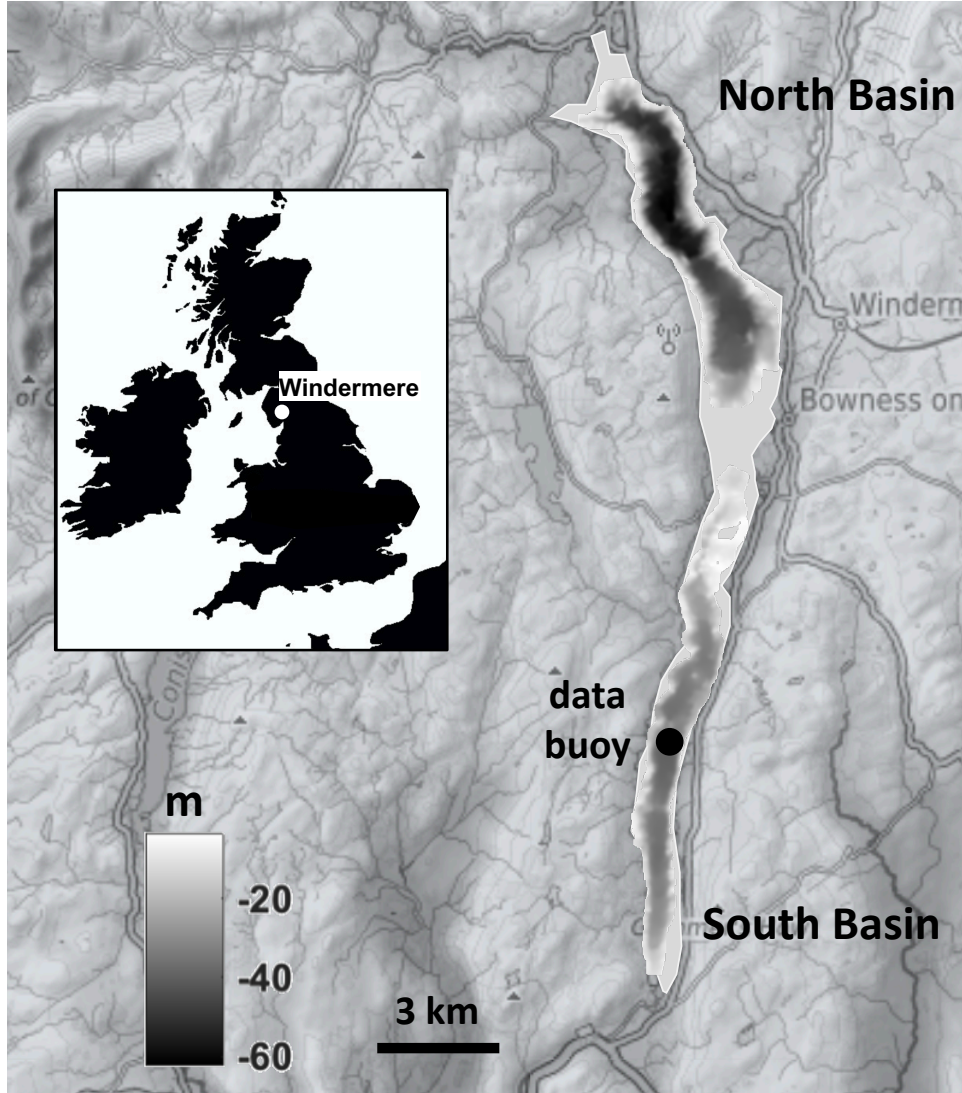


Figure 3: Location and bathymetry of Windermere, with CEH data buoy location also shown.

Table 2: Best parameter set for three different relative water depths (h/H) obtained by minimising NSE .

h/H	RMSE ($^{\circ}C$)	RMAE (%)	NSE	Kz_{max}	C	η
0	0.688	7.6	0.973	5.60e-05	0.9000	0.3111
0.5	0.657	6.9	0.971	6.70e-05	0.1000	1.3667
1.0	0.732	8.5	0.963	1.00e-04	0.1000	1.1556

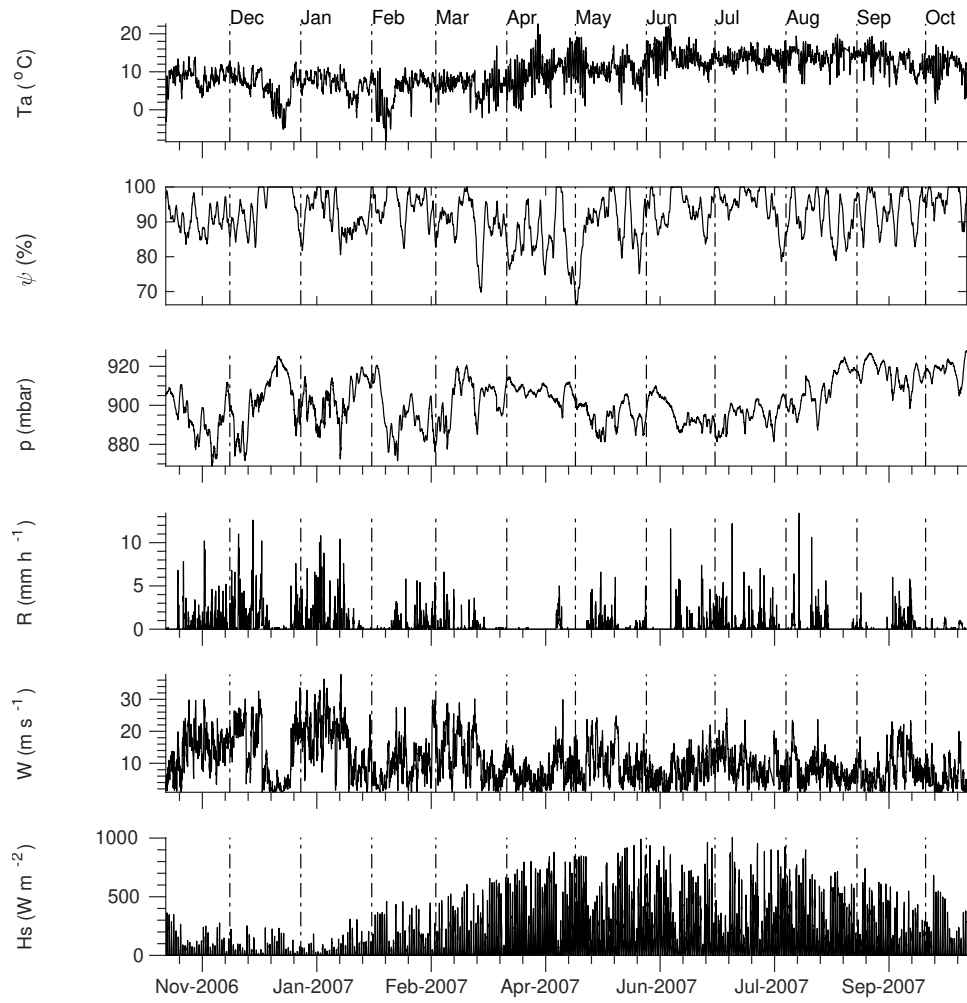


Figure 4: Hourly-averaged meteorological data series used in the model calibration. T_a = air temperature; ψ = relative humidity, p = atmospheric pressure; R = hourly rainfall; W = windspeed at a height of 2 m above the water surface; and H_s = short wave irradiance at the water surface.

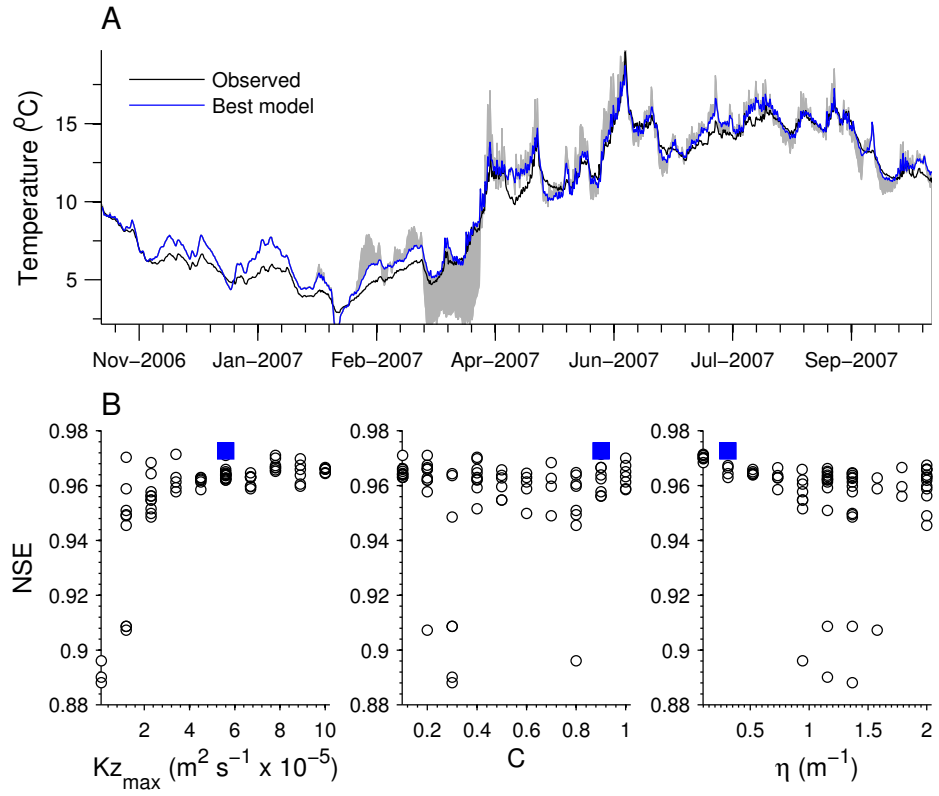


Figure 5: a) Comparison between observed water temperature, T_w , at the surface (black line), modelled T_w for different parameter sets (grey envelope), and the best model simulation (blue line) for which $NSE = 0.973$. b) NSE vs. Kz_{max} , C and η . Blue squares represent the optimal parameter values.

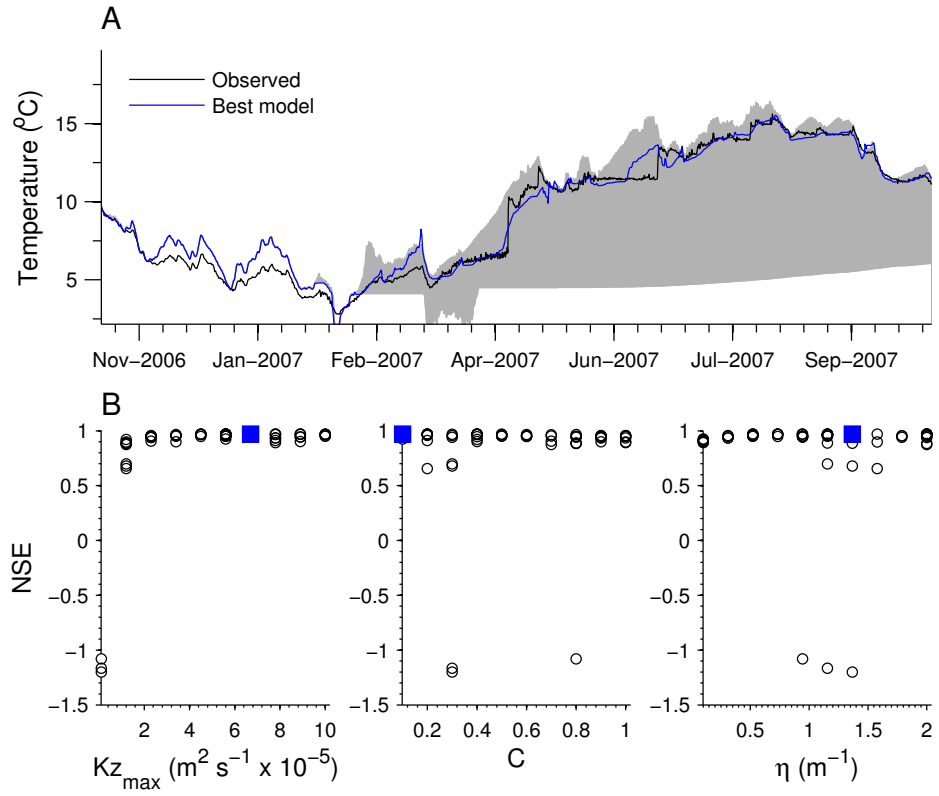


Figure 6: a) Comparison between observed water temperature, T_w , at mid-depth (black line), modelled T_w for different parameter sets (grey envelope), and the best model simulation (blue line) for which $NSE = 0.971$. b) NSE vs. Kz_{max} , C and η . Blue squares represent the optimal parameter values.

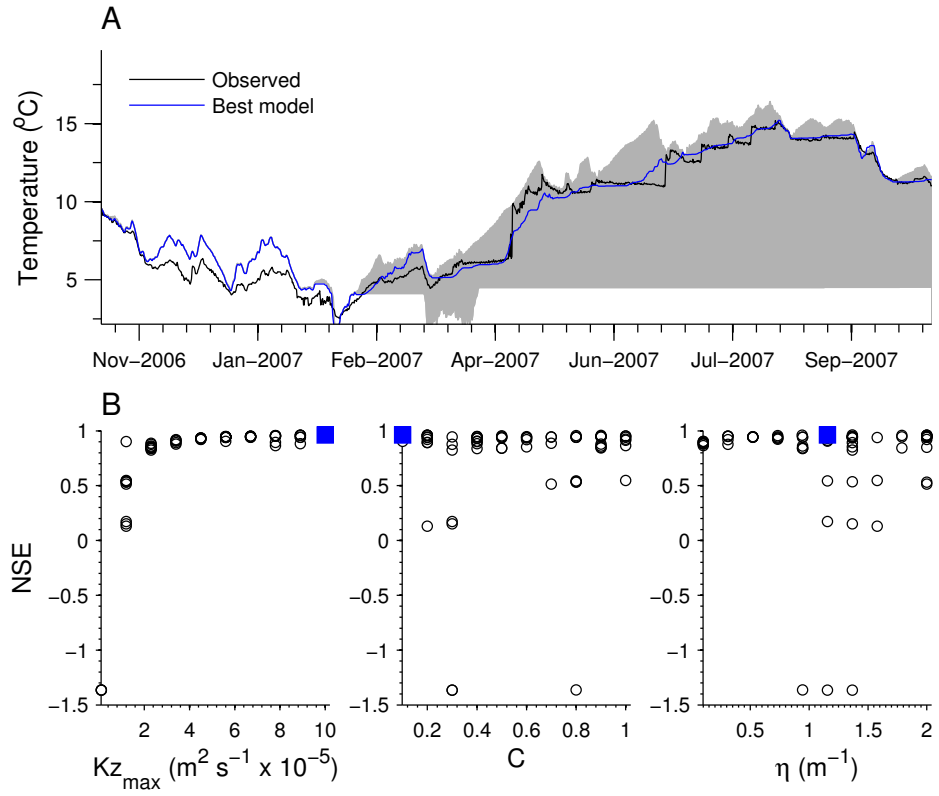


Figure 7: a) Comparison between observed water temperature, T_w , at the bottom (black line), modelled T_w for different parameter sets (grey envelope), and the best model simulation (blue line) for which $NSE = 0.963$. b) NSE vs. Kz_{max} , C and η . Blue squares represent the optimal parameter values.

an alternative, we use a different formulation:

$$\bar{T}e(t) = \frac{1}{Nlayers} \sum_{i=1}^{Nlayers} Te_i \quad (13)$$

where $\bar{T}e$ is a simple vertical averaging of the temperature profile.

Choosing the optimum data set values using this approach yields good performance for the weighted vertical water temperature (Table 3). It is encouraging that a single run (run 54) gives optimal values of each of the three metrics (RMSE, RMAE, and NSE). Figure 8 compares the simulated temperature series (broken lines) using the best parameter set ($Kz_{max} = 8.90 \times 10^{-5}$, $C = 0.20$ and $\eta = 2.00$) against the observed temperature values (solid lines) at five different relative water depths (h/H) at intervals of $h/H = 0.25$. Overall model performance is very good with a value of $NSE = 0.979$.

Although performance is very good for all the top five model runs (Table 3), it is notable that all the values for Kz_{max} are above 5.0×10^{-5} , close to its upper bound, and the values of C are ≤ 0.2 . The high turbulence intensity generated by the strong wind forcing necessitates a high value of Kz_{max} , with the aim of controlling the energy diffusion through the water column correctly.

Work by Hondzo and Stefan (1993) on small lakes has established that C is function of the lake area (or, more specifically, of the maximum fetch). The small surface area of Llyn Conwy would suggest a value of $C = 0.11$, which coincides with the results reported in Table 3. On the other hand, due to the fact that the wind velocities were measured on a buoy located at around 90% of the fetch for the dominant southwesterly winds, an overestimation of the wind velocity values is implicit in the measurement, because wind velocity typically increases with the fetch (Young and Verhagen, 1996). This implies that the further the wind measurement is made along the fetch, the smaller the value of C .

Multiple relationships of the form $\eta = az_{sd}^{-b}$, where z_{sd} is the sechi disk depth in metres, and a and b are constants that typically take values of 1.5 and 1.0 respectively, were derived to estimate η (Henderson-Sellers, 1984; Hondzo and Stefan, 1993). Using a mean value of $z_{sd} = 1.8$ determined from field measurements at Llyn Conwy, gives a value of $\eta = 1.1 \text{ (m}^{-1}\text{)}$. This is significantly lower than the value that emerges from the optimal parameter value set ($\eta = 2.0 \text{ (m}^{-1}\text{)}$) but similar to the second and third best parameter sets (Table 3).

5.2. Sensitivity Analysis

To provide further insights into how water temperature responds to variation in the model parameters, a time-dependent sensitivity quantity (S_i) was computed for each parameter as:

$$S_i = \frac{|Te_i^{up} - Te_i^{lo}|}{Te_i^{best}} \quad (14)$$

where the subscript i indicates a time instant, Te_i^{up} is the temperature simulated with the upper bound value of the parameter, Te_i^{lo} is the temperature simulated

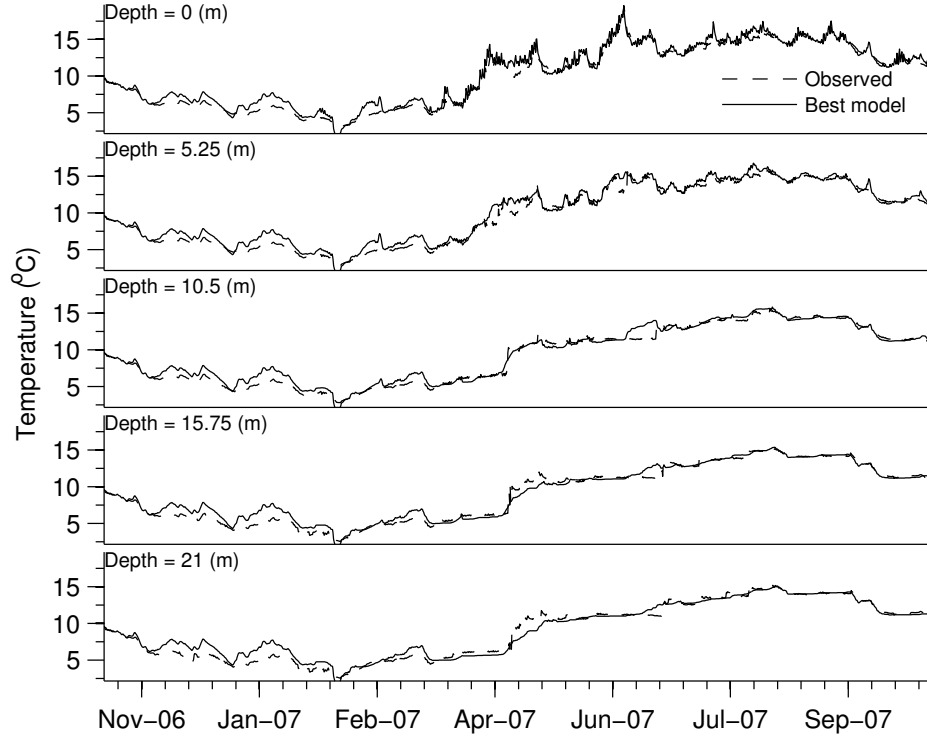


Figure 8: Comparison between simulated and observed water temperature at five depths (every 20% of the water depth from the surface to the bottom), for the best parameter set (run 54; Table 3).

Table 3: Best five parameter sets for depth-averaged model performance. Bold values indicate the best parameter values and their performance metrics.

Run	RMSE ($^{\circ}C$)	RMAE (%)	NSE	Kz_{max}	C	η
54	0.7092	6.48	0.9785	8.90e-05	0.2000	2.0000
11	0.7160	6.51	0.9782	7.80e-05	0.1000	1.1556
46	0.7196	6.51	0.9776	8.90e-05	0.1000	0.9400
55	0.7311	6.53	0.9775	7.80e-05	0.2000	0.7333
30	0.7396	6.56	0.9775	6.70e-05	0.1000	1.3667

Table 4: Average sensitivity, S_i , for each calibration parameter at the surface ($h/H = 0.0$) and mid-depth ($h/H = 0.5$).

% h/H	S_i (%) for		
	Kz_{max}	C	η
0.0	5.87	1.35	6.79
0.5	46.99	2.84	52.52

with the lower bound parameter value and Te_i^{best} is the temperature simulated with the best parameter set. Higher values of S_i indicate greater parameter sensitivity.

Figures 9 and 10 summarise the sensitivity analysis for water temperature at the surface and at mid-depth. Comparing the respective values for S_i (see Table 4), it is clear that water temperature at mid-depth is much more sensitive to model parameter values, especially in spring and summer. The main reason for this is that the uppermost layers are more sensitive to changing weather conditions, such that temperature variations are driven most of the time by the heat flux (Kn) at the water surface. The accuracy of the temperature prediction at the epilimnion thus depends strongly on the quality of the meteorological data. On the other hand, temperatures in the layers below the mixed layer are strongly influenced by how the turbulent energy, represented by Kz , and the downward distribution of the remaining incoming solar radiation (Hz) are parameterised. This is demonstrated in Figures 10a) and 10c), which show the model results to be very sensitive to Kz_{max} and η and that model uncertainty is greatest at lower levels of the water column.

The model becomes much less sensitive to the choice of parameter values from mid-autumn to late-winter. This period is characterised by low incoming heat energy and stronger winds that drive a constant convective circulation (Morales-Marín et al., 2017). The high values and a homogeneous distribution of Kz guarantees constant mixing throughout the water depth. It follows that the thermal structure in these periods is most sensitive to changes in weather conditions.

Water temperature has a low sensitivity to C most of the time. Relatively high values of S_i for both surface and mid-depth layers between mid-February and late-March coincide with the beginning of the seasonal increase in Hz , and with a slight decline in wind speeds. This is effectively a transition period between a wind-dominated state with weak stratification to another in which the heat fluxes play a significant role in allowing stratification. As the kinematic energy transferred from the wind is affected by C , such transitions increase the uncertainty in the chosen of a value for C . This also causes difficulties in the way that the model estimates the temperature, which is observable in the difference between the simulated and the measured values in the top graphs in Figures 9b and 10b.

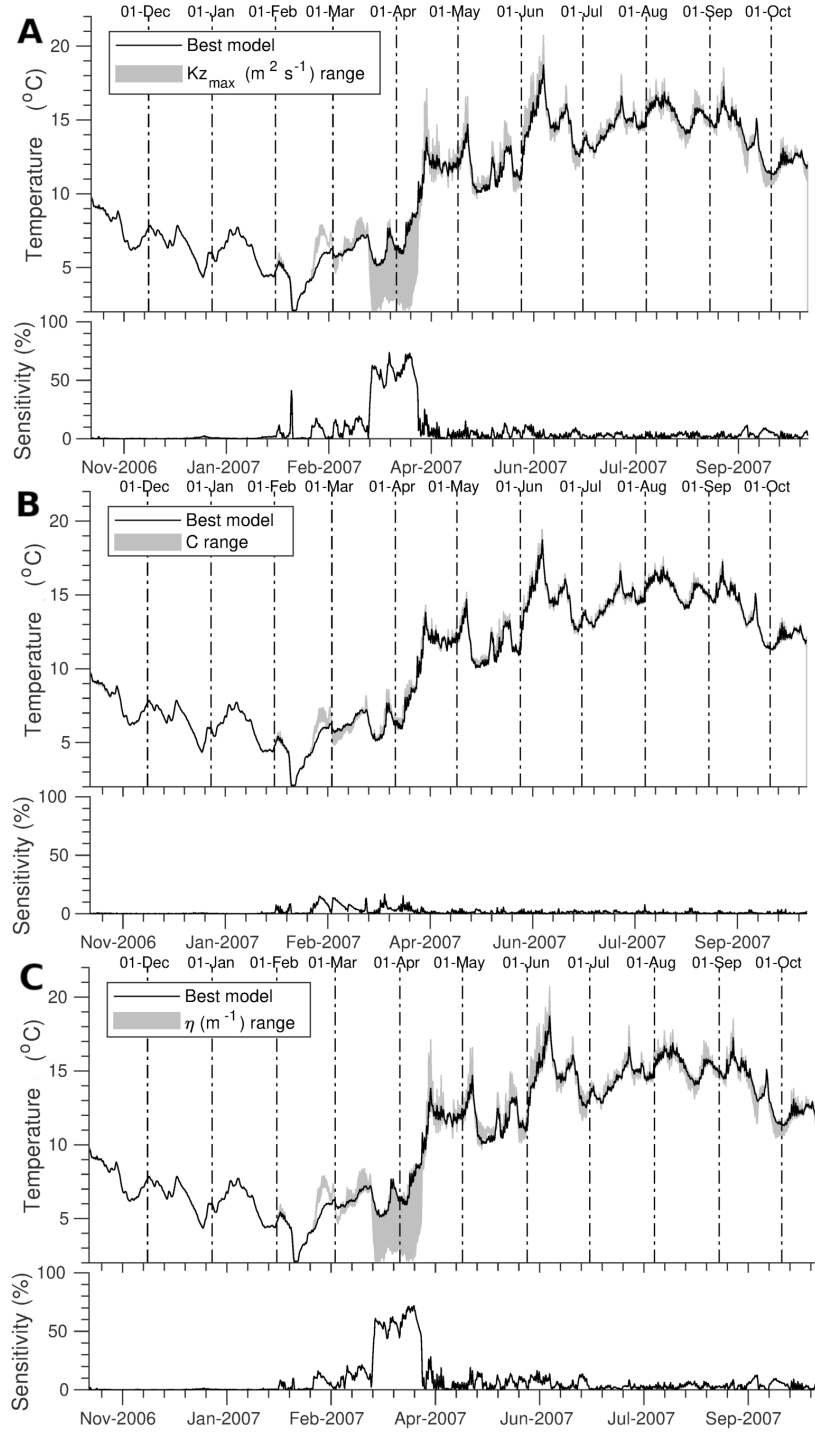


Figure 9: Sensitivity analysis for water temperatures at the surface for a) Kz_{max} , b) C and c) η . Comparison of observations, best model simulation, and the range of model simulations for the upper and lower parameter limits. Sensitivity index (S_i) estimated using Equation 14 is also shown.

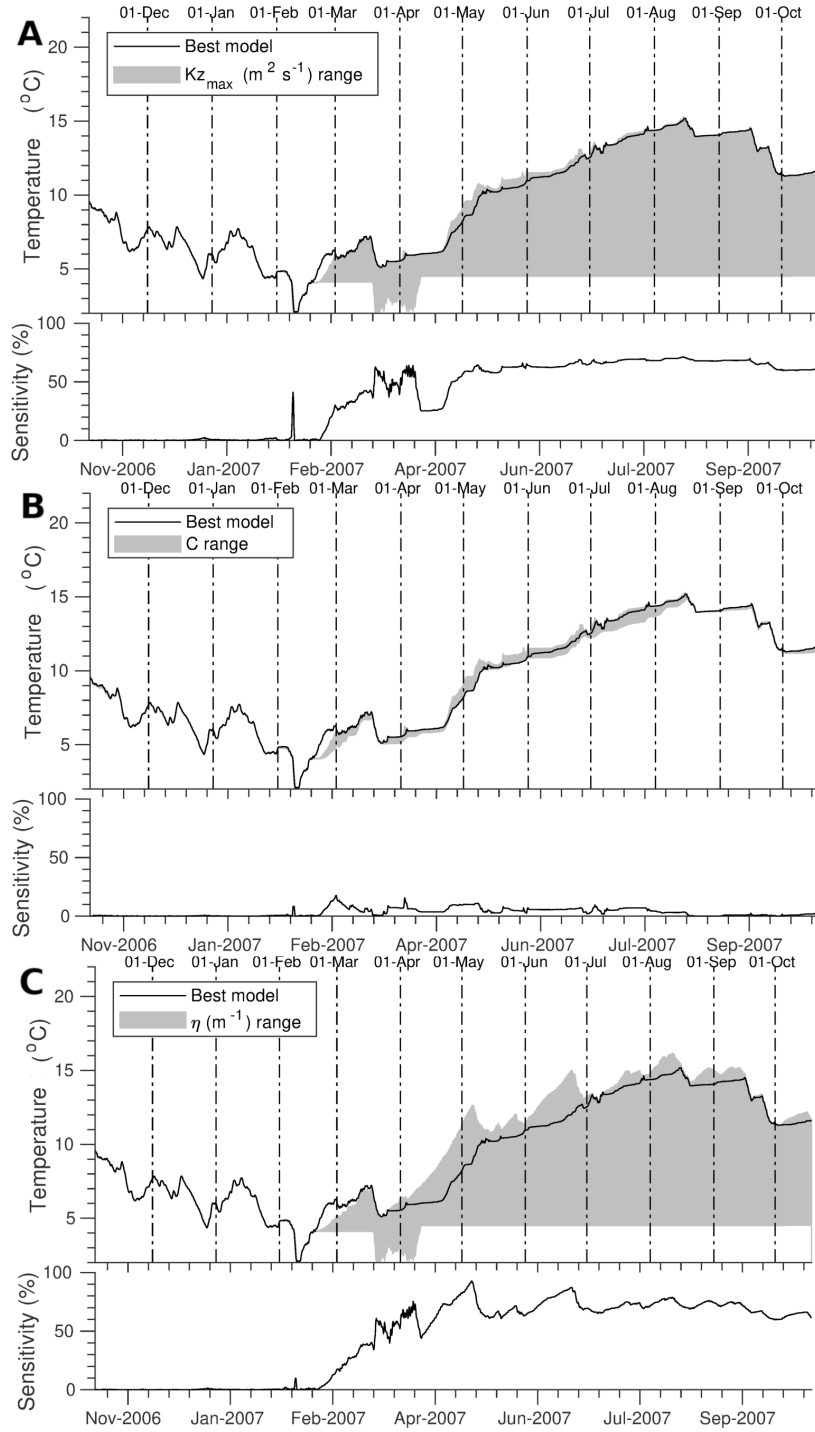


Figure 10: Sensitivity analysis for water temperatures at mid-depth for a) Kz_{max} , b) C and c) η . Comparison of observations, best model simulation, and the range of model simulations for the upper and lower parameter limits. Sensitivity index (S_i) estimated using Equation 14 is also shown.

5.3. Validation

Validation against observations for January to December 2008 using the best set of calibrated parameter values (run 54 from Table 3) gave a good agreement between observed and the simulated temperature, with NSE values of 0.951, 0.972 and 0.973 at the water surface, mid-depth and at the bottom respectively (Figure 11a). Temperature profiles at different times (Figure 11b) similarly demonstrate the ability of the model to represent the vertical structure throughout the year. A maximum difference of $3.9\text{ }^{\circ}\text{C}$ occurs during the first half of February where the mean RMSE is $0.74\text{ }^{\circ}\text{C}$ and the mean RMAE is 8.1% for the 24 profiles plotted and $<10\%$ for 77% of the 12-month validation period.

To test the effect of the choice of the model time step, UCLAKE was set up using daily averaged meteorological data, except for the solar irradiation where a single value corresponding to the midday value was taken. The analysis showed that the maximum temperature differences between observed and simulated decrease to $1.7\text{ }^{\circ}\text{C}$ with a decrease in the RMSE to $0.69\text{ }^{\circ}\text{C}$ and in the RMAE to 6.1%. Of course, when a daily time step is used, sub-daily details of the vertical structure are not resolved.

Other sources of error are related to the uncertainty of the meteorological forcing data. Small changes in air temperature affect the temperature structure, especially in the mixed layer. Likewise, changes in wind forcing trigger changes in the flux of heat by evaporation, and therefore in the net heat balance at the water surface. Small increases in wind speed can cause a deepening of the mixed layer and changes in the temperature structure at the hypolimnion. It is therefore important that the meteorological datasets are rigorously acquired and screened for quality.

5.4. Thermal stratification

Meteorological forcings are the main driver of hydrodynamics in Llyn Conwy. In autumn and winter, low incoming solar radiation and high wind speeds (mean 12.7 m s^{-1}) ensure that the lake is well mixed around 68% of the time (Figure 12). During early spring, lower wind speeds allow the lake to stratify for 44% of the time. In the validation year, March and April are characterised by intermittent overturns of the thermal structure due to irregular variation of the wind speed and the onset of a more sustained air temperature rise. In late April and early May, the lake becomes stratified with a more-or-less constant mixed layer depth of 2.5 m. Later in May, stronger winds deepen the mixed layer to 15 m. The lake is stratified for about 80% of the time in summer. Episodic mixing occurs due to windy conditions such that the mixing depth extends to the bottom at various times between late May and the end of August (Figure 12c).

5.5. Illustrative simulation of multi-decadal thermal structure

Analysis of the GLDAS annually-averaged meteorological data for this region of Wales reveals significant trends in most of the forcing variables. Air temperatures show warming at a rate of $0.009\text{ }^{\circ}\text{C yr}^{-1}$ ($0.44\text{ }^{\circ}\text{C}$ over the period 1948-2000).

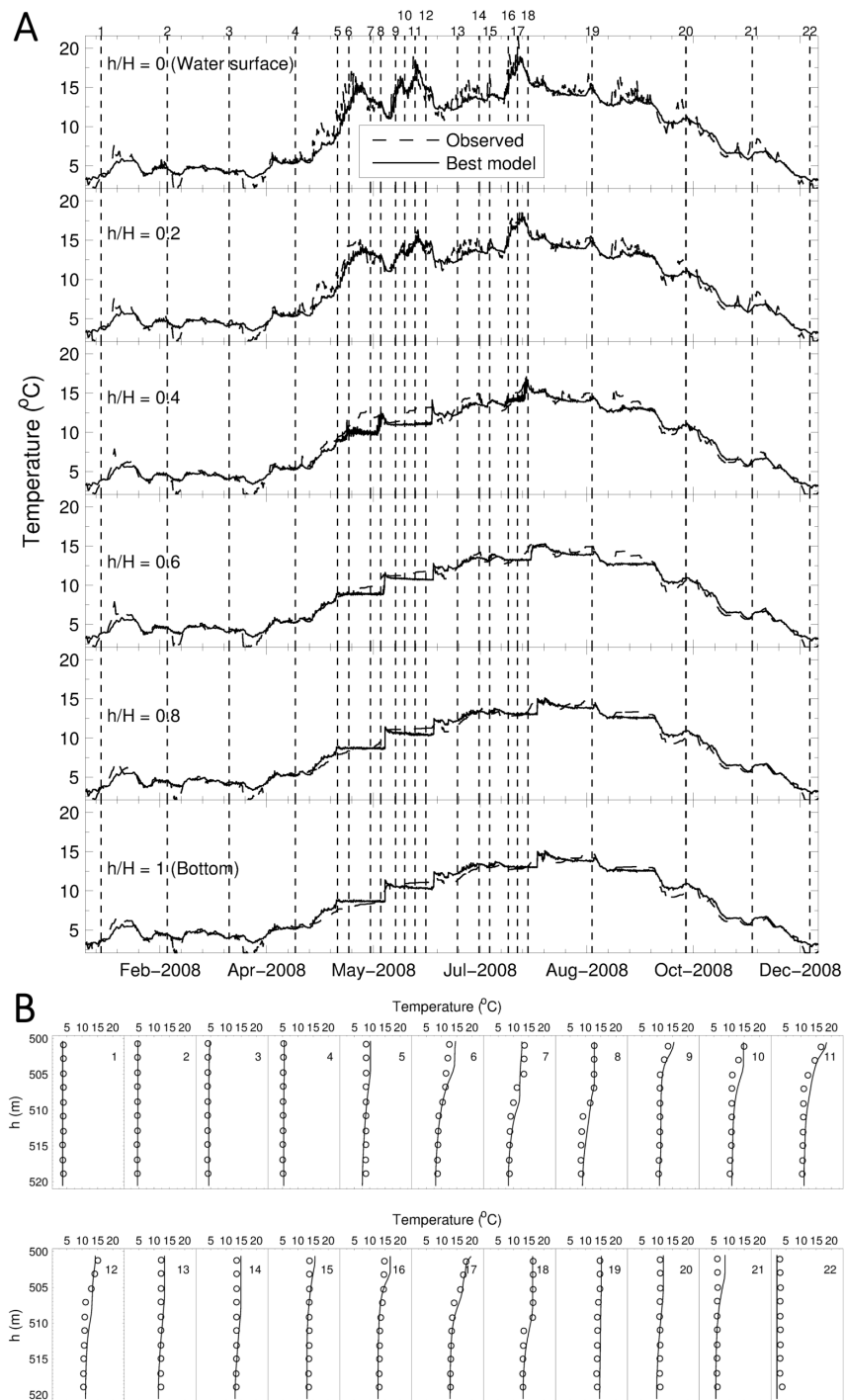


Figure 11: a) Comparison between best simulated (continuous line) and observed temperature (dashed line) at different relative depths from the surface to the bottom. Vertical dashed lines show times of b) observed (empty circles) and simulated (continuous line) water temperature profiles.

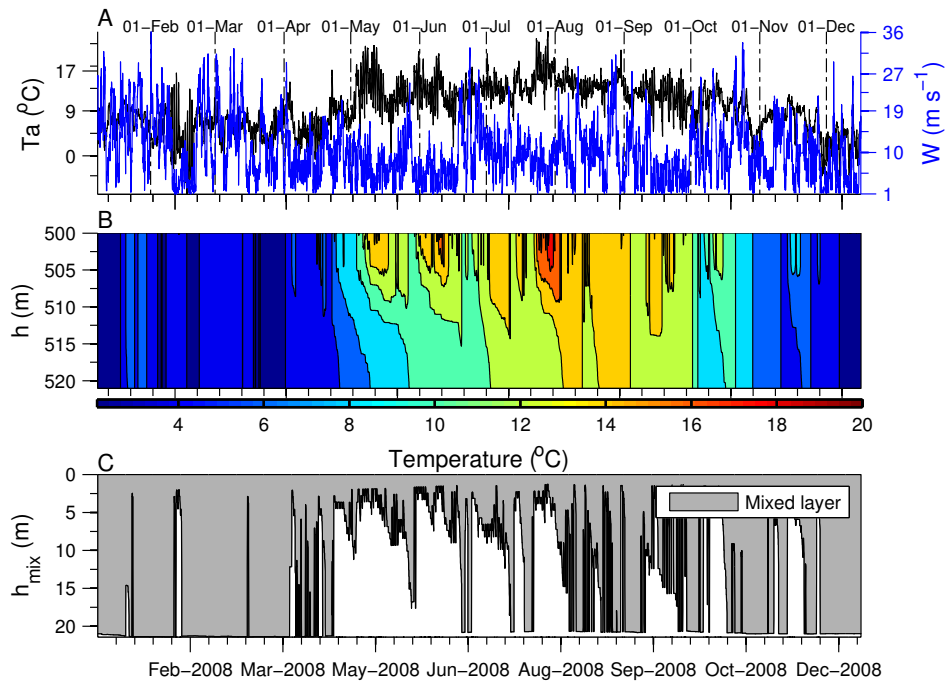


Figure 12: a) Time series for dominant meteorological forcing variables air temperature (black) and wind velocity (blue); b) simulated water temperature contours; c) simulated mixed layer depth.

This warming shows decadal variation, with a slight cooling 1950-1960, followed by warming after 1960, and a more rapid warming 1990-2000. Mean annual wind speed has increased at a rate $0.01 \text{ m s}^{-1} \text{ yr}^{-1}$ (p-value = 0.01) during the same period.

Simulated annually-averaged water temperatures in Llyn Conwy also show warming trends. Depth-averaged temperatures (Figure 13a) show an increase of $0.0042 \text{ }^{\circ}\text{C yr}^{-1}$. However, the trend varies within the water column. The temperature trend at the epilimnion (Figure 13b) and at the metalimnion (Figure 13c) is $0.0044 \text{ }^{\circ}\text{C yr}^{-1}$ (effectively tracking air temperature). In contrast, the hypolimnion (Figure 13d) warms at a rate of just $0.0020 \text{ }^{\circ}\text{C yr}^{-1}$. The 1980-2000 warming trend has been more pronounced and sustained, especially in the upper lake layers. A period of lake cooling followed by a period of constant temperature between 1960 and 1980 is also observed in all three layers. Cooling of the lower layers is lagged and attenuated with respect to that of the epilimnion.

This exploratory multi-decadal analysis of the depth-averaged water temperature reveals clear seasonal differences in warming trend. During summer, the lake is exposed to high incoming solar radiation and air temperatures, and low albedo, which drives warming at $0.011 \text{ }^{\circ}\text{C yr}^{-1}$ (see Figure 14c). In spring, the warming trend is weaker at $0.007 \text{ }^{\circ}\text{C yr}^{-1}$, influenced by the antecedent water temperature conditions from the preceding winter. Water temperatures are also relatively stable

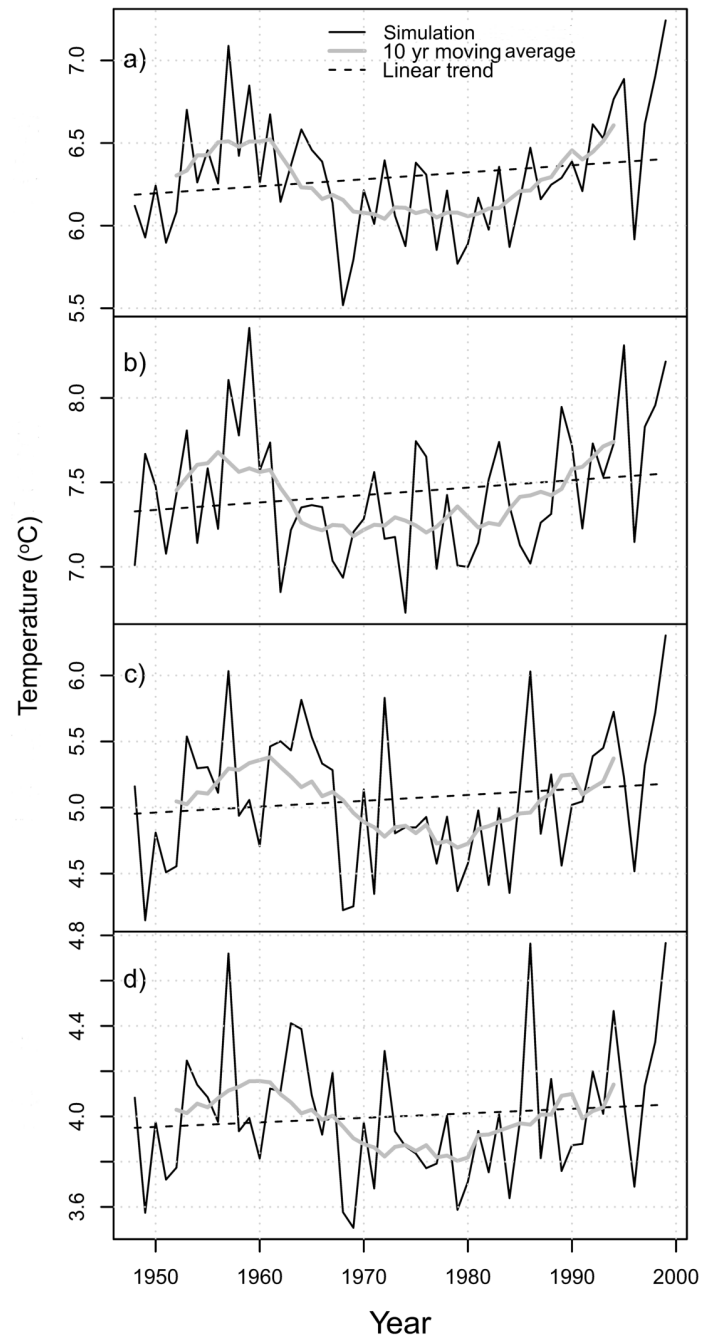


Figure 13: Multi-decadal UCLAKE simulation of annual-average water temperature, with 10-year moving average and linear trend for: a) water column average, b) epilimnion, c) metalimnion and d) hypolimnion.

during summer and spring, around median values of 10.55 °C and 3.75 °C respectively, with a no significant outliers. In contrast, the autumn and winter show a very subtle cooling trend of $-0.00025\text{ °C yr}^{-1}$ (see Figure 14a) and $-0.0025\text{ °C yr}^{-1}$ (Figure 14d) respectively. Confidence limits of water temperature in winter are relatively narrow and around the median (2.18 °C) since the homothermal structure remains unchanged most of the time. A few relatively warm months in 1952 and 1996 are outliers in the analysis.

Although there is no evidence of a statistically significant trend in the depth of the mixed layer, 10-year moving average water temperatures (Figure 15a) and mixed-layer depth show opposing behaviours. During periods of lake warming, the mixed layer gets thinner (reaching an average of about 12 m), whereas during cooling it thickens to 13 m. Disaggregation into monthly-averaged mixed-layer depths (Figure 15b) shows the lake to be fully stratified in June, July and August when the mixed layer is fairly constant at 2 m approximately, whereas a homothermal condition occurs during winter months. Spring and autumn are transitions when the mixed layer depth shows a large variance around the median, with a significant number of outliers represented by weak stratification events following windless episodes accompanied by sustained solar radiation.

5.6. Deep lake performance: Windermere case study

UCLAKE parameters for Windermere were adjusted manually based on the previous experience acquired during the model calibration for Llyn Conwy. The resulting preliminary model results indicate that the model reproduces the observed water temperature series at all water depths, simulating the peaks and the timing of the lake stratification correctly (Figure A.18). As with the Llyn Conwy application, UCLAKE performs better here for the upper layers, for which $\text{NSE} > 0.9$ and $\text{PBIAS} = 2\%$. Larger discrepancies between observed and simulated water temperatures are found at the hypolimnion where model performance is reduced to $\text{NSE} = 0.75$. In terms of systematic bias, at some layers the model tends to underestimate water temperature and at some other level the model overestimates it. This additional study shows that the capabilities of UCLAKE are not restricted to very shallow systems but also extend to deeper lakes. The Windermere application was constrained by data availability, and represents a challenging case for a 1D scheme given that the separate north basin, as well as inflows and outflows, have been neglected here.

6. Discussion

6.1. Model calibration and validation

Most 1D lake models have been implemented to simulate relatively short-term lake dynamics using daily-averaged meteorological data (e.g., Hondzo and Stefan, 1993; Bell et al., 2006). On the other hand, many lakes, especially in upland locations, experience marked sub-daily changes in meteorological conditions. The

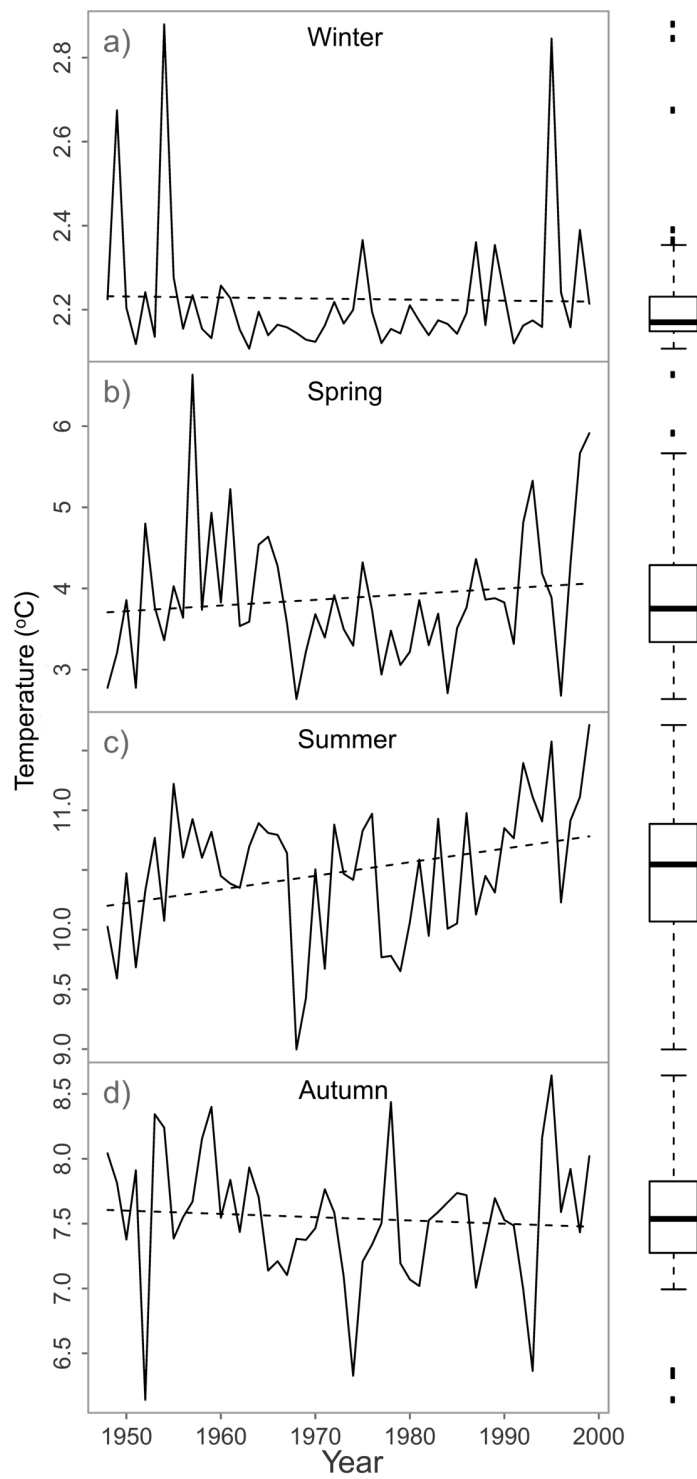


Figure 14: Seasonal water-depth averaged temperature time-series and boxplots for: a) winter, b) spring, c) summer and d) autumn.

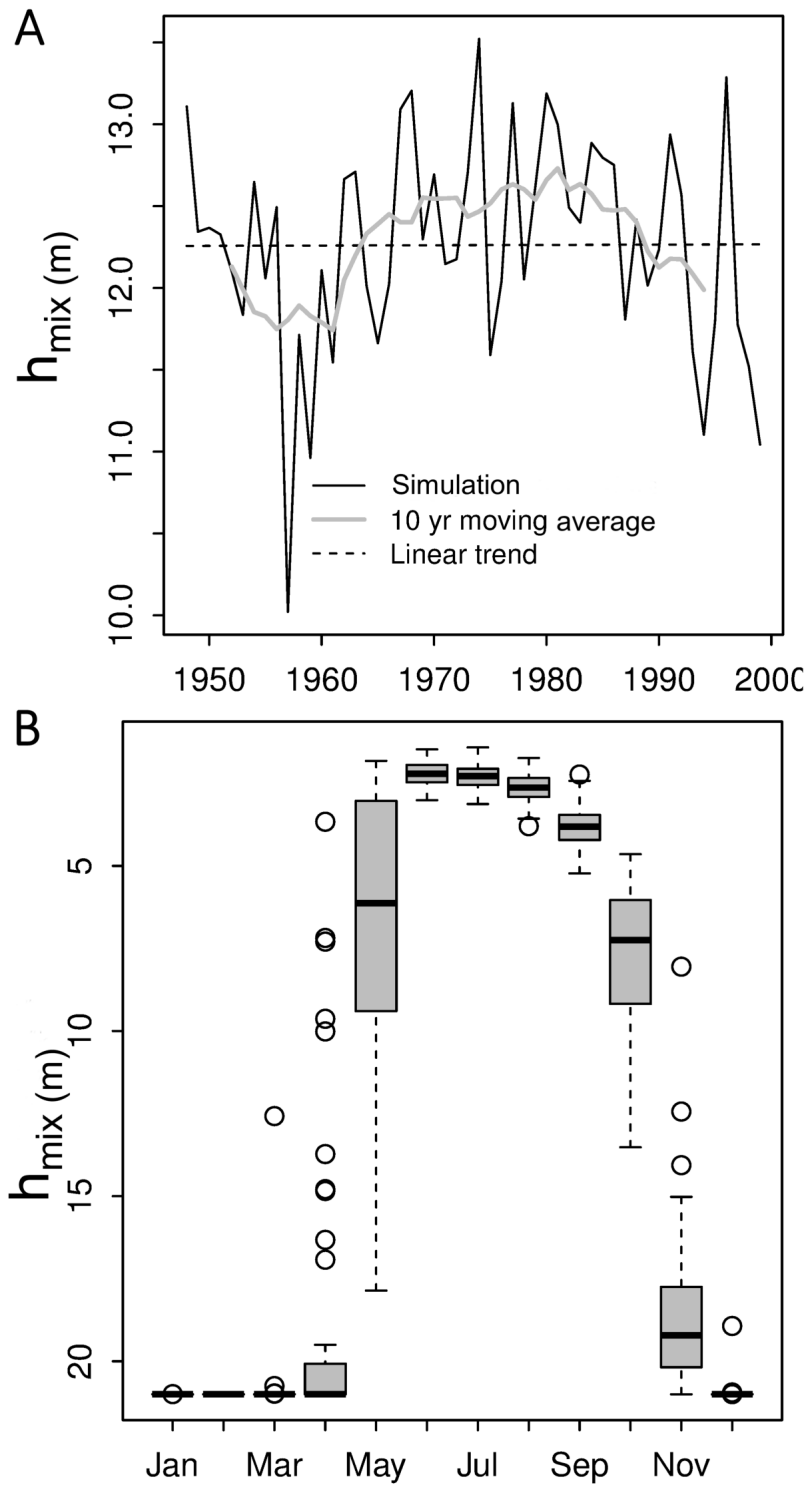


Figure 15: a) Simulated annual-average mixed-layer depth, with 10-year moving averaged water temperature and fitted linear trend and b) boxplots of simulated monthly mixed-layer depth.

energetic wind regimes typical of upland locations can also create numerical instability problems. UCLAKE, has been developed to allow computationally efficient investigation of lake thermal structure at a wider range of time scales, from sub-daily behaviour to multi-decadal trends, taking advantage of a flexible simulation time step and adaptive numerical time step that ensures stability at all times.

Calibration of UCLAKE can be based on the most appropriate temperature information for the problem at hand. The use of hourly temperature profiles (not reported in detail here) yielded different and heterogeneous sets of parameter values at each time, although their values show homogeneity when aggregated by month or season. This approach was not considered practical because of the difficulties in grouping parameters (which also affects the parsimony of the model), and calibration based on water temperature time series was adopted in order to obtain an unique value for each unconstrained parameter. Calibration for the Llyn Conwy case study resulted in generally excellent performance, with $NSE = 0.97$ and $RMSE = 0.71$ °C for $Kz_{max} = 8.90 \times 10^{-5}$, $C = 0.2$ and $\eta = 2.0$ of 80 model simulations. Similar procedures applied by Hondzo and Stefan (1993) to calibrate a 1D model for a range of small lakes yielded an RMSE of 1.1 °C. Trial and error calibration of a 1D model of a reservoir by Bonnet et al. (2000), where the parameters were divided into three different groups: heat exchange, dispersion processes and inflow and outflows discharges, yielded an RMSE of 0.57 °C.

The validation performance of UCLAKE is also very good with $NSE > 0.95$ for surface, mid-depth and bottom layer water temperature time series in the Llyn Conwy case. Comparisons between observed and simulated water temperature profiles yield an average RMAE of 8.1%, and $RMAE < 10\%$ for 77% of the validation period. A high RMAE of 50% was found for some short periods in winter when the lake is well-mixed and the water temperature falls to ≈ 4 °C. To deal with such low water temperatures, some models (e.g., Hondzo and Stefan, 1991) include a threshold below which the model is not able to make any temperature estimation. In other energy-budget models (Imberger and Patterson, 1981; Spigel et al., 1986), the time step is adapted within a range from 0 to 24 h as a function of sub-daily water-surface energy balance, and the temperature of inflow and outflow. Other sources of discrepancies between observed and simulated temperatures especially at the epilimnetic layers are probably due to uncertainty in the determination of air and dew point temperature (Hondzo and Stefan, 1992). Inaccurate or unrepresentative wind forcing information is another source of temperature errors, because most of the components of the heat energy balance at the water surface depend on it (Gal et al., 2003).

The implementation of a UCLAKE model for the south basin of Windermere, using previously calibrated parameters for Llyn Conwy, showed similarly good performance, with $NSE > 0.9$ for upper layers with and around 0.75 for lower half layers. This study case demonstrate the ability of the model to simulate thermal structures in deeper and larger lakes subjected to different meteorological forcing conditions. Future work will extend the application of UCLAKE to a wider range of lakes located in other climatic and geographic regions. An ice-cover sub-model

is currently being incorporated to facilitate this.

6.2. *Exploratory simulation of multi-decadal thermal structure*

A 52-year simulation of water temperatures in an upland lake demonstrates the ability of UCLAKE to efficiently model longer-term lake behaviour and response to environmental variability and change. Previous studies have related climate change to a warming trend in lakes (e.g., Robertson and Ragotzkie, 1990; Flaim et al., 2016). Trends in simulated water temperatures in Llyn Conwy indicate more rapid warming of the upper and middle layers than the bottom layer, where the warming trend is much weaker. This is consistent with earlier studies (e.g., Robertson and Ragotzkie, 1990; Hondzo and Stefan, 1991, 1993) suggest that the temperature at water surface and medium-depth layers varies linearly with air temperature, with stronger responses in summer and in spring. The relationship between air and water temperature at the epilimnion is affected by the time resolution at which a particular model run. In Lake Zurich, Switzerland, distinct differences in the relationship between minimum and mean daily air temperature and daily water temperature highlighted the need to model the diurnal cycle (Livingstone, 2003). Doing so takes into account possible diurnal asymmetries of the forcing variables, specially air temperature. Because of its ability to run at an hourly time step, UCLAKE captures the diurnal cycle of forcing variables necessary to accurately resolve their net effect on lake temperature.

7. Conclusions

UCLAKE provides a robust and computationally efficient platform for 1D simulation of lake thermal structure and the behaviour of the mixed layer at a wide range of time scales. UCLAKE is able to simulate lake thermal structure for lakes of different size and depths subjected to different meteorological conditions. Its adaptive time step ensures numerical stability under a wide range of forcing conditions and support for both sub-daily and daily time steps allows it to capture lake dynamics at a wide range of timescales.

Given of the difficulties in acquiring long-term lake observations of vertical temperature variation, numerical models such as UCLAKE allow generation of synthetic lake temperature time series from readily available meteorological data and a simple representation of lake bathymetry. Because of the physical basis of the model, calibration should be robust across lakes with similar climatology and morphology, although re-calibration will clearly be necessary where these differ. Multi-decadal hindcast simulation forced by downscaled GLDAS-derived meteorological variables can show how lakes are likely to be responding to climate change. Results for a case study upland lake are consistent with observational studies elsewhere that show attenuated responses at depth and season-specific trends that are masked by annually-averaged observations.

8. Acknowledgements

Monitoring of Llyn Conwy was supported by the CEH Source to Sea and Carbon Catchment projects, and the present study was partly supported by NERC (NE/I007520/1 - UKLEON). The first author acknowledges UCL Department of Geography for the award of a PhD scholarship. We gratefully acknowledge provision of UK Meteorological Office MIDAS Land Surface Observations data via the British Atmospheric Data Centre and thank the Centre of Ecology and Hydrology (CEH) at Bangor for allowing access to AWS data for Llyn Conwy. Bathymetry data for Windermere were kindly supplied by Dr Simon Turner in the UCL Environmental Change Research Centre.

9. References

References

- Adrian, R., O'Reilly, C.M., Zagarese, H., Baines, S.B., Hessen, D.O., Keller, W., Livingstone, D.M., Sommaruga, R., Straile, D., Van Donk, E., Weyhenmeyer, G.A., Winder, M., 2009. Lakes as sentinels of climate change. *Limnology and Oceanography* 54, 2283–2297. doi:10.4319/lo.2009.54.6_part_2.2283.
- Antonopoulos, V., Gianniou, S., 2003. Simulation of water temperature and dissolved oxygen distribution in Lake Vegoritis, Greece. *Ecological Modelling* 160, 39–53.
- Austin, J.A., Coleman, S.M., 2007. Lake superior summer temperatures are increasing more rapidly than regional air temperatures: a positive ice-albedo feedback. *Geophysical Research Letters* 34, L06604.
- Austnes, K., Evans, C., Eliot-Laze, C., Naden, P., Old, G., 2010. Effects of storm events on mobilisation and in-stream processing of dissolved organic matter (DOM) in a Welsh peatland catchment. *Biogeochemistry* 99, 157–173.
- Bell, V., George, D., Moore, R., Parker, J., 2006. Using a 1-D mixing model to simulate the vertical flux of heat and oxygen in a lake subject to episodic mixing. *Ecological Modelling* 190, 41–54.
- Beven, K., Freer, J., 2001. Equifinality, data assimilation, and uncertainty estimation in mechanistic modelling of complex environmental systems using the glue methodology. *Journal of Hydrology* 249, 11–29.
- Bonnet, M., Poulin, M., Devaux, J., 2000. Numerical modeling of thermal stratification in a lake reservoir. methodology and case study. *Aquatic Sciences-Research Across Boundaries* 62, 105–124.

- Burchard, H., Bolding, K., Kuehn, W., Meister, A., Neumann, T., Umlauf, L., 2006. Description of a flexible and extendable physical-biogeochemical model system for the water column. *Journal of Marine Systems* 61, 180–211. doi:10.1016/j.jmarsys.2005.04.011. Workshop on Future Directions in Modelling Physical-Biological Interactions (WKFDPI 2004), Barcelona, Spain.
- Cohen, A.S., Gergurich, E.L., Kraemer, B.M., McGlue, M.M., McIntyre, P.B., Russel, J.M., Simmons, J.D., Swarzenski, P., 2016. Climate warming reduces fish production and benthic habitat in Lake Tanganyika, one of the most biodiverse freshwater ecosystems. *Proceedings of the National Academy of Sciences, USA* 113, 9563–9568.
- Dokulil, M.T., Jagsch, A., George, G.D., Anneville, O., Jankowski, T., Wahl, B., Lenhart, B., Blenckner, T., Teubner, K., 2006. Twenty years of spatially coherent deepwater warming in lakes across Europe related to the North Atlantic Oscillation. *Limnology and Oceanography* 51, 2787–2793. doi:10.4319/lo.2006.51.6.2787.
- Fang, G., Yang, J., Chen, Y., Zammit, C., 2015. Comparing bias correction methods in downscaling meteorological variables for a hydrologic impact study in an arid area in China. *Hydrology and Earth System Sciences* 19, 2547–2559.
- Flaim, G., Eccel, E., Zeileis, A., Toller, G., Cerasino, L., Obertegger, U., 2016. Effects of re-oligotrophication and climate change on lake thermal structure. *Freshwater Biology* 61, 1802–1814.
- Ford, D., Stefan, H., 1980. Thermal predictions using integral energy model. *Journal of the Hydraulics Division* 106, 39–55.
- Gal, G., Imberger, J., Zohary, T., Antenucci, J., Anis, A., Rosenberg, T., 2003. Simulating the thermal dynamics of Lake Kinneret. *Ecological Modelling* 162, 69–86.
- Glanz, D., Orlob, G., Young, G., 1973. *Ecologic simulation: Tocks Island Lake*. Water Resources Engineers, inc.
- Goudsmit, G.H., Burchard, H., Peeters, F., Wüest, A., 2002. Application of $k - \epsilon$ turbulence models to enclosed basins: The role of internal seiches. *Journal of Geophysical Research: Oceans* 107, 3320.
- Hampton, S.E., Izmet'Eva, L.R., Moore, M.V., Katz, S.L., Dennis, B., Silow, E.A., 2008. Sixty years of environmental change in the world's biggest freshwater lake - Lake Baikal, Siberia. *Global Change Biology* 14, 1947–1958.
- Henderson-Sellers, B., 1984. *Engineering Limnology*. Pitman Advanced Pub. Program (Boston).

- Henderson-Sellers, B., 1985. New formulation of eddy diffusion thermocline models. *Applied Mathematical Modelling* 9, 441–446.
- Hipsey, M., Bruce, L., Hamilton, D., 2014. GLM - General Lake Model: model overview and user information. AED Report No.26. The University of Western Australia, Perth, Australia .
- Hondzo, M., Stefan, H., 1992. Propagation of uncertainty due to variable meteorological forcing in lake temperature models. *Water Resources Research* 28, 2629–2638.
- Hondzo, M., Stefan, H., 1993. Lake water temperature simulation model. *Journal of Hydraulic Engineering* 119, 1251.
- Hondzo, M., Stefan, H.G., 1991. Three case studies of lake temperature and stratification response to warmer climate. *Water Resources Research* 27, 1837–1846.
- Hostetler, S.W., Bates, G.T., Giorgi, F., 1993. Interactive coupling of a lake thermal model with a regional climate model. *Journal of Geophysical Research: Atmospheres* 98, 5045–5057.
- Huber, W., Harleman, D., 1968. Laboratory and analytical studies of the thermal stratification of reservoirs. Massachusetts Institute of Technology, Hydrodynamics Laboratory.
- Imberger, J., Patterson, J., 1981. A dynamic reservoir simulation model-DYRESM: 5, in: Fisher, H. (Ed.), *Transport Models for Inland and Coastal Waters*. Academic Press, pp. 310–361.
- Jones, I., Feuchtmayr, H., 2017. Data from automatic water monitoring buoy from Windermere south basin, 2008 to 2011. NERC Environmental Data Centre. doi:<https://doi.org/10.5285/bd37710e-6a53-49f0-9a07-6973408a3342>.
- Kraemer, B.M., Anneville, O., Chandra, S., Dix, M., Kuusisto, E., Livingstone, D.M., Rimmer, A., Schladow, S.G., Silow, E., Sitoki, L.M., Tamatamah, R., Vadeboncoeur, Y., McIntyre, P.B., 2015. Morphometry and average temperature affect lake stratification responses to climate change. *Geophysical Research Letters* 42, 4981–4988. doi:10.1002/2015GL064097.
- Livingstone, D.M., 2003. Impact of secular climate change on the thermal structure of a large temperate central European lake. *Climatic Change* 57, 205–225.
- Livingstone, D.M., Dokulil, M.T., 2001. Eighty years of spatially coherent austrian lake surface temperatures and their relationship to regional air temperature and the North Atlantic Oscillation. *Limnology and Oceanography* 46, 1220–1227.
- Mironov, D., Heise, E., Kourzeneva, E., Ritter, B., Schneider, N., Terzhevik, A., 2010. Implementation of the lake parameterisation scheme, FLake, into the

- numerical weather prediction model COSMO. *Boreal Environment Research* 15.
- Mooij, W.M., Trolle, D., Jeppsen, E., Arhonditsis, G., Belolipetsky, P.V., Deonatus, B., Chitamwebwa, R., 2010. Challenges and opportunities for integrating lake ecosystem modelling approaches. *Aquatic Ecology* 44, 633–667.
- Morales-Marín, L.A., French, J.R., Burningham, H., 2017. Implementation of a 3D ocean model to understand upland lake wind-driven circulation. *Environmental Fluid Mechanics* 17, 1255–1278. doi:10.1007/s10652-017-9548-6.
- Morales-Marin, L.A., French, J.R., Burningham, H., Battarbee, R.W., 2017. Three-dimensional hydrodynamic and sediment transport modeling to test the sediment focusing hypothesis in upland lakes. *Limnology and Oceanography* 63, 156–176. doi:10.1002/lno.10729.
- Munk, W., Anderson, E., 1948. Notes on a theory of the thermocline. *Journal of Marine Research* 3, 276–295.
- Nakamura, Y., Hayakawa, N., 1991. Modelling of thermal stratification in lakes and coastal seas. 20 th General Assembly of the International Union of Geodesy and Geophysics, Vienna, Austria, 08/11-24/91 , 227–236.
- Nash, J., Sutcliffe, J., 1970. River flow forecasting through conceptual models. *Journal of Hydrology* 83, 307–335.
- O'Reilly, C.M., Sharma, S., Gray, D.K., Hampton, S.E., Read, J.S., Rowley, R.J., Schneider, P., Lenters, J.D., McIntyre, P.B., Kraemer, B.M., Weyhenmeyer, G.A., Straile, D., Dong, B., Adrian, R., Allan, M.G., Anneville, O., Arvola, L., Austin, J., Bailey, J.L., Baron, J.S., Brookes, J.D., de Eyto, E., Dokulil, M.T., Hamilton, D.P., Havens, K., Hetherington, A.L., Higgins, S.N., Hook, S., Izmet'eva, L.R., Joehnk, K.D., Kangur, K., Kasprzak, P., Kumagai, M., Kuusisto, E., Leshkevich, G., Livingstone, D.M., MacIntyre, S., May, L., Melack, J.M., Mueller-Navarra, D.C., Naumenko, M., Noges, P., Noges, T., North, R.P., Plisnier, P.D., Rigosi, A., Rimmer, A., Rogora, M., Rudstam, L.G., Rusak, J.A., Salmaso, N., Samal, N.R., Schindler, D.E., Schladow, S.G., Schmid, M., Schmidt, S.R., Silow, E., Soylu, M.E., Teubner, K., Verburg, P., Voutilainen, A., Watkinson, A., Williamson, C.E., Zhang, G., 2015. Rapid and highly variable warming of lake surface waters around the globe. *Geophysical Research Letters* 42, 10,773–10,781. doi:10.1002/2015GL066235.
- Orlob, G., Selna, L., 1970. Temperature variations in deep reservoirs. *Journal of the Hydraulics Division* 96, 391–410.
- Patrick, S., Stevenson, A., 1986. Palaeoecological evaluation of the recent acidification of Welsh lakes Part 3; Llyn Conwy and Gamallt, Gwynedd. Technical Report 19. Palaeoecology Research Unit, University College London.

- Patten, B., Egloff, D., Richardson, T., et al., 1975. Total ecosystem model for a cove in Lake Texoma. Academic Press.
- Penman, H., 1948. Natural evaporation from open water, bare soil and grass. *Proceedings Royal Society of London A* 193, 120–145.
- Perroud, M., Goyette, S., Martynov, A., Beniston, M., Annevillec, O., 2009. Simulation of multiannual thermal profiles in deep Lake Geneva: A comparison of one-dimensional lake models. *Limnology and Oceanography* 54, 1574–1594. doi:10.4319/lo.2009.54.5.1574.
- Press, W.H., Teukolsky, S.A., Vetterling, W.T., Flannery, B.P., 2007. *Numerical Recipes 3rd Edition: The Art of Scientific Computing*. 3 ed., Cambridge University Press, New York, NY, USA.
- Riley, M., Stefan, H., 1988. MINLAKE: A dynamic lake water quality simulation model. *Ecological Modelling* 43, 155–182.
- Robertson, D., Ragotzkie, R., 1990. Changes in the thermal structure of moderate to large sized lakes in response to changes in air temperature. *Aquatic Sciences-Research Across Boundaries* 52, 360–380.
- Rodell, M., Houser, P., Jambor, U., Gottschalck, J., Mitchell, K., Meng, C., Arsenault, K., Cosgrove, B., Radakovich, J., Bosilovich, M., et al., 2004. The global land data assimilation system. *Bulletin of the American Meteorological Society* 85, 381–394.
- Rösner, R., Mueller-Navarra, D.C., Zorita, E., 2012. Trend analysis of weekly temperatures and oxygen concentrations during summer stratification in Lake Plüßee: A long-term study. *Limnology and Oceanography* 57, 1479–1491. doi:10.4319/lo.2012.57.5.1479.
- Ryan, P., Harleman, D., 1973. An analytical and experimental study of transient cooling pond behavior. volume 161. Ralph M. Parsons Laboratory for Water Resources and Hydrodynamics, Massachusetts Institute of Technology.
- Saloranta, T., Andersen, T., 2007. MyLake—A multi-year lake simulation model code suitable for uncertainty and sensitivity analysis simulations. *Ecological Modelling* 207, 45–60.
- Spigel, R.H., Imberger, J., Rayner, K.N., 1986. Modeling the diurnal mixed layer. *Limnology and Oceanography* 31, 533–556.
- Themeßl, M.J., Gobiet, A., Heinrich, G., 2012. Empirical-statistical downscaling and error correction of regional climate models and its impact on the climate change signal. *Climatic Change* 112, 449–468.

- Valerio, G., Pilotti, M., Barontini, S., Leoni, B., 2015. Sensitivity of the multianual thermal dynamics of a deep pre-alpine lake to climatic change. *Hydrological processes* 29, 767–779.
- Vinçon-Leite, B., Lemaire, B.J., Khac, V.T., Tassin, B., 2014. Long-term temperature evolution in a deep sub-alpine lake, lake bourget, france: how a one-dimensional model improves its trend assessment. *Hydrobiologia* 731, 49–64.
- Winslow, L.A., Read, J.S., Hansen, G.J.A., Rose, K.C., Robertson, D.M., 2017. Seasonality of change: summer warming rates do not fully represent the effects of climatic change on lake temperatures. *Limnology and Oceanography* 62, 2168–2178.
- Woolway, R.I., Dokulil, M.T., Marszelewski, W., Schmid, M., Bouffard, D., Merchant, C.J., 2017. Warming of Central European lakes and their response to the 1980s climate regime shift. *Climatic Change* 142, 505–520. doi:10.1007/s10584-017-1966-4.
- Woolway, R.I., Jones, I.D., Maberly, S.C., French, J.R., Livingstone, D.M., Monteith, D.T., Simpson, G.L., Thackeray, S.J., Andersen, M.R., Battarbee, R.W., et al., 2016. Diel surface temperature range scales with lake size. *PloS one* 11, e0152466.
- Woolway, R.I., Merchant, C.J., 2018. Intralake heterogeneity of thermal responses to climate change: A study of large northern hemisphere lakes. *Journal of Geophysical Research: Atmospheres* 123, 3087–3098.
- Wu, J., 1982. Wind-stress coefficients over sea surface from breeze to hurricane. *Journal of Geophysical Research* 87, 9704–9706.
- Yao, H., Samal, N.R., Joehnk, K.D., Fang, X., Bruce, L.C., Pierson, D.C., Rusak, J.A., James, A., 2014. Comparing ice and temperature simulations by four dynamic lake models in Harp Lake: past performance and future predictions. *Hydrological Processes* 28, 4587–4601.
- Young, I., Verhagen, L., 1996. The growth of fetch limited waves in water of finite depth. Part 1. Total energy and peak frequency. *Coastal Engineering* 29, 47–78.
- Zhong, Y., Notaro, M., Vavrus, S.J., 2019. Spatially variable warming of the Laurentian great lakes: an interaction of bathymetry and climate. *Climate Dynamics* 52, 5833–5848.

Appendix A. Model comparison

Table A.5: Comparison of two 1D lake dynamic models, GLM and UCLAKE.

		Model	
		GLM	UCLAKE
Code			
- Language		C. Requires Intel compilers and NetCDF lib.	C. Compiled with GNU or Intel compilers.
- Source		Open source	Open source
Input data			
- Time step		Sub-hourly	Sub-hourly adaptive
- Met. Forcing data		Air temperature, precipitation, relative humidity, incoming solar radiation, cloudiness, wind speed and pressure	Air temperature, precipitation, relative humidity, incoming solar radiation, wind speed and pressure
- Lake morphology		Lagrangian layer structure. Layers expand and contract dynamically	Lagrangian layer structure. Layers expand and contract dynamically
Output data			
- Format		NetCDF, ascii	ascii
- Variables		Temperature, density, salinity	Temperature, density
- Vertical resolution		< 10 layers	any number of layers
- Temporal resolution		at time steps	at time steps
Approach			
- Approach		Energy budget	Eddy diffusivity
- Processes		Inflow and outflows, mixing, surface heating and cooling and ice processes. Snow and ice modelling.	- Inflow and outflows, mixing, surface heating and cooling. Ice cover model under development
- Parameters for calibration		8 mixing efficiency parameters and 3 bulk aerodynamic coefficients.	1 turbulent diffusion coefficient, 1 wind sheltering coefficient and 1 extinction coefficient
Performance on a single 3.4GHz Intel i7-3770 core		4.2 min per year of simulation	3.8 min per year of simulation

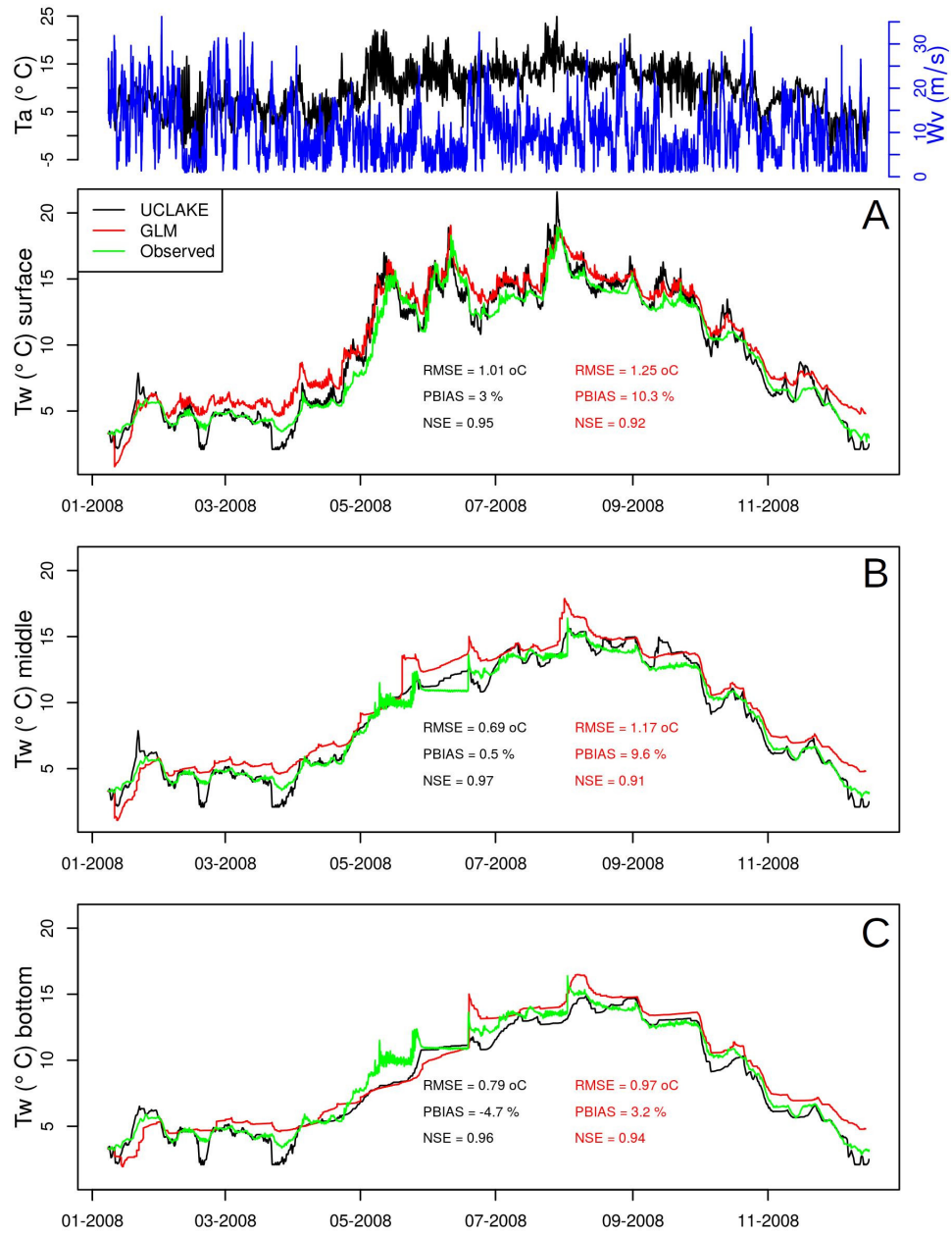


Figure A.16: Comparison of hourly observed and estimated water temperatures using UCLAKE and GLM at a) surface, b) middle depth and c) bottom for Llyn Conwy. Air temperature and wind speed are shown in the top panel.

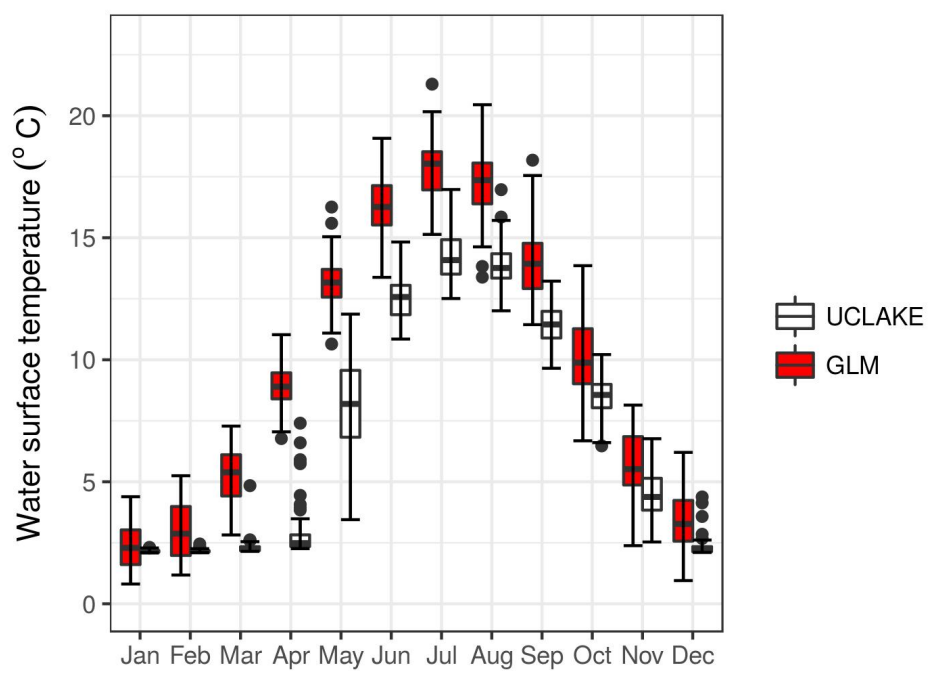


Figure A.17: Monthly box plots of Llyn Conway water surface temperatures estimated using UCLAKE and GLM for the period 1948-2000.

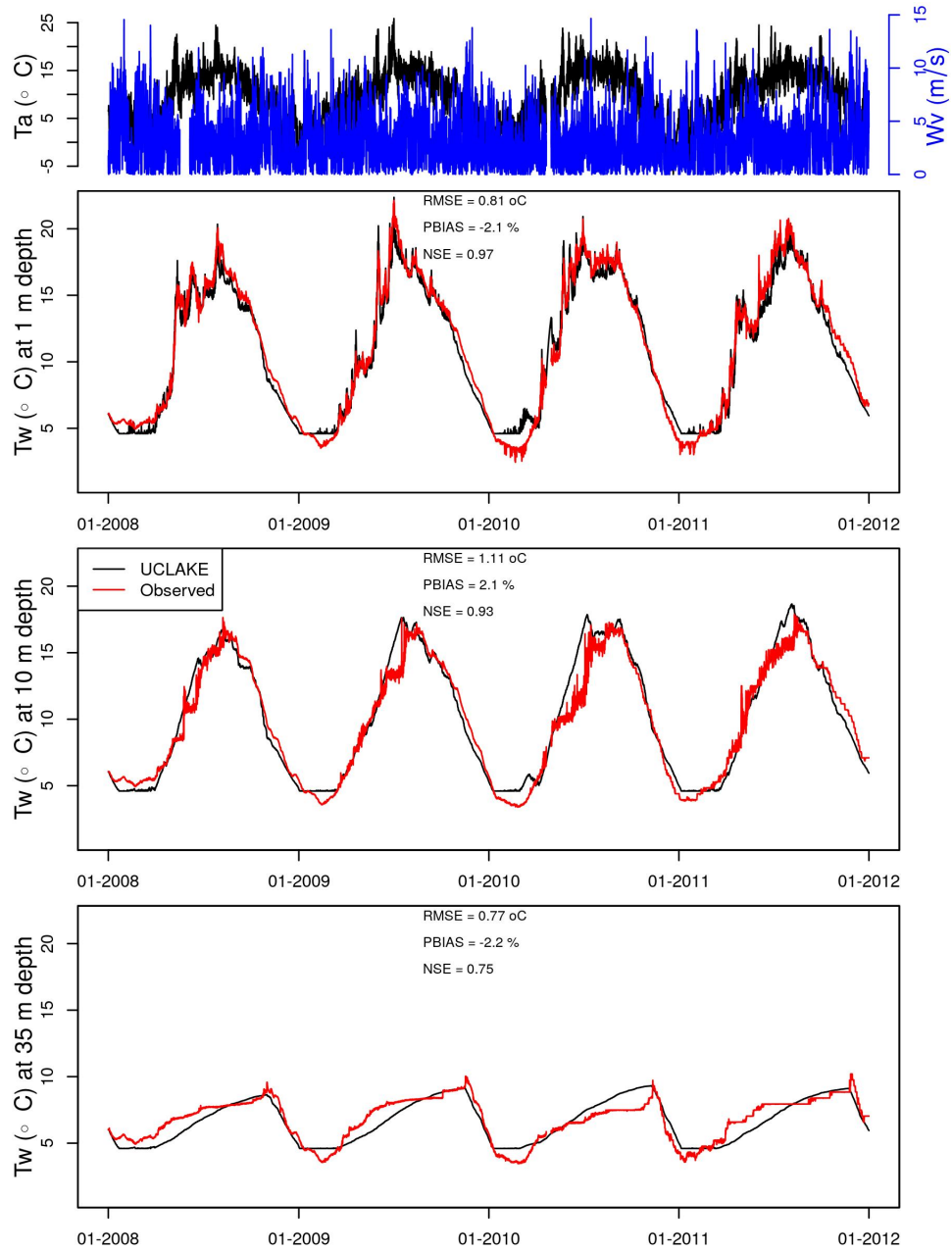


Figure A.18: Hourly water temperatures (T_w) in Windermere simulated at 1 m, 10 m and 35 m water depths from 2008 - 2012. The top panel shows hourly air temperature (T_a) and wind speed (W_v) for the same period.